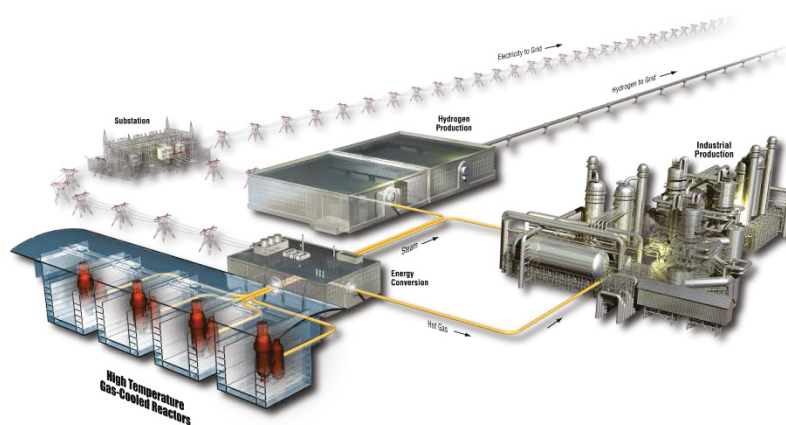# IAEA Coordinated Research Project on HTGR Physics, Thermal-Hydraulics, and Depletion Uncertainty Analysis

Prismatic HTGR Benchmark Definition: Phase I

G. Strydom
F. Bostelmann

September 2015

IAEA Coordinated Research Project on HTGR Physics, Thermal-Hydraulics, and Depletion Uncertainty Analysis

Prismatic HTGR Benchmark Definition: Phase I

G. Strydom
F. Bostelmann

September 2015

Idaho National Laboratory
INL ART TDO Program
Idaho Falls, Idaho 83415

http://www.inl.gov

IAEA Coordinated Research Project on HTGR Physics, Thermal-Hydraulics, and Depletion Uncertainty Analysis

Prismatic HTGR Benchmark Definition: Phase I

INL/EXT-15-34868
Revision 1

September 2015

Author:

_____   9/14/2015
G. Strydom   Date
R&D Scientist: Nuclear Science and Technology

Approved by:

_____   9/09/2015
Hans D. Gougar   Date
INL ART TDO Deputy Director

_____   9/15/15
Diane V. Croson   Date
INL ART TDO Deputy Director

_____   9/10/2015
Daren K. Jensen   Date
INL ART TDO Quality Assurance

CONTRIBUTORS

Name	Organization	Country	Role
Gerhard Strydom	Idaho National Laboratory	USA	Prismatic Reactors Working Group Coordinator, Specifications Developer
Friederike Bostelmann	Gesellschaft für Reaktorsicherheit	Germany	Specifications Developer, Technical Reviewer
Winfried Zwermann	Gesellschaft für Reaktorsicherheit	Germany	Technical Reviewer
Victor Boyarinov	National Research Centre Kurchatov Institute	Russia	Technical Reviewer
Frederik Reitsma	International Atomic Energy Agency (IAEA)	Austria	IAEA Coordinated Research Project (CRP) Coordinator
Kostadin Ivanov	Pennsylvania State University	USA	CRP on HTGR Uncertainty Analysis in Modeling Coordinator

FOREWORD

In February 2009, the Technical Working Group on Gas-Cooled Reactors recommended that the proposed International Atomic Energy Agency's Coordinated Research Project on the High-Temperature Gas-Cooled Reactor Uncertainty Analysis in Modeling be implemented.

This document contains the prismatic Phase I benchmark specification for the uncertainty analysis in modeling. The specification includes the prismatic high-temperature reactor design description, exercise definitions, support data, and reporting templates for Phase I.

REVISION HISTORY

This is the first public-access release of this document under the Idaho National Laboratory (INL) document system, and future updates will be reflected in the revision number. The Phase I specification was released in two earlier draft formats (in 2013 and 2014), as well as a major update before the second Research Coordination Meeting workshop in December 2014. The first INL-numbered version (INL/LTD-15-34868, Rev. 0) was released to a limited group of benchmark participants in early 2015, reflecting feedback provided at the Research Coordination Meeting. For this update, it was decided to release the document with the same number to the public domain for wider benchmark participation.

A summary of significant changes made compared with previous draft versions is contained in Appendix E. This is a major revision, and all Modular High-Temperature Gas-Cooled Reactor 350 exercises will require updates of previous results. No changes were made to the VHTRC and Exercise I-3 and I-4 specifications.

CONTENTS

FIGURES

TABLES

ACRONYMS

BP	burnable poison
CRP	Coordinated Research Project
CZP	cold zero power
ENDF	Evaluated Nuclear Data File
HFP	hot full power
HTGR	high-temperature gas-cooled reactor
HTTR	High-Temperature Engineering Test Reactor
IAEA	International Atomic Energy Agency
INL	Idaho National Laboratory
KAERI	Korea Atomic Energy Research Institute
LBP	lumped burnable poison
LWR	light water reactor
MHTGR	modular high-temperature gas-cooled reactor
ND	number density
NDL	nuclear data library
NEA	Nuclear Energy Agency
NSC	Nuclear Science Committee
OECD	Organization for Economic Cooperation and Development
ORNL	Oak Ridge national Laboratory
RCM	Research Coordination Meeting
SA	sensitivity analysis
SiC	silicon carbide
TRISO	tri-structural isotropic
UA	uncertainty analysis
UAM	uncertainty analysis in modeling
$UC_{0.5}O_{1.5}$	uranium carbide oxide
USA	United States of America
VHTR	very-high-temperature reactor
VHTRC	Very-High-Temperature Reactor Critical

IAEA Coordinated Research Project on HTGR Physics, Thermal-Hydraulics, and Depletion Uncertainty Analysis

Prismatic HTGR Benchmark Definition: Phase I

1. INTRODUCTION

The continued development of high-temperature gas-cooled reactors (HTGRs) requires verification of HTGR design and safety features with reliable high-fidelity physics models and robust, efficient, and accurate codes.

The predictive capability of coupled-neutronics/thermal-hydraulics and depletion simulations for reactor design and safety analysis can be assessed with sensitivity analysis (SA) and uncertainty analysis (UA) methods. Uncertainty originates from errors in physical data, manufacturing uncertainties, modelling, and computational algorithms. (The interested reader is referred to the large body of published SA and UA literature for a more complete overview of the various types of uncertainties, methodologies, and results obtained.)

SA is helpful for ranking the various sources of uncertainty and error in the results of core analyses. SA and UA are required to address cost, safety, and licensing needs, and should be applied to all aspects of reactor multi-physics simulation. SA and UA can guide experimental, modeling, and algorithm research and development. Current SA and UA rely either on derivative-based methods, such as stochastic sampling methods, or on generalized perturbation theory to obtain sensitivity coefficients. Neither approach addresses all needs.

To benefit from recent advances in modeling and simulation and the availability of new covariance data (nuclear data uncertainties), extensive sensitivity and uncertainty studies are needed for quantification of the impact of different sources of uncertainties on the design and safety parameters of HTGRs. Only a parallel effort in advanced simulation and in nuclear data improvement will be able to provide designers with more robust and well-validated calculation tools to meet design target accuracies.

In February 2009, the Technical Working Group on Gas-Cooled Reactors of the International Atomic Energy Agency (IAEA) recommended that the proposed Coordinated Research Project (CRP) on the HTGR Uncertainty Analysis in Modeling (UAM) be implemented. This CRP is a continuation of the previous IAEA and Organisation for Economic Cooperation and Development (OECD)/Nuclear Energy Agency (NEA) international activities on verification and validation of available analytical capabilities for HTGR simulation for design and safety evaluations [1,2,3]. Within the framework of these activities different numerical and experimental benchmark problems were performed, and insight was gained about specific physics phenomena and the adequacy of analysis methods.

The CRP will also benefit from interactions with the currently ongoing OECD/NEA Light Water Reactor (LWR) UAM benchmark activity [4] by taking into consideration the peculiarities of HTGR designs and simulation requirements. Because the prismatic design specification included in this document is based directly on the OECD/NEA Modular High-Temperature Gas-Cooled Reactor (MHTGR)-350 MW benchmark [5], participants in both activities can leverage their core models developed for the OECD/NEA benchmark for this CRP benchmark with only minor changes.

The next section introduces the main objectives of the HTGR UAM benchmark.

1.1 Objective of the CRP

SA and UA methods need to be considered as an integral part of the development of coupled code methods. Of particular importance are innovative methods that address nonlinearity, which can predict the

probability distributions in output parameters, treat discrete events, and handle simultaneously large input data and response fields in a computationally efficient manner.

In the proposed comprehensive IAEA CRP on HTGR UAM, different SA and UA methods will be compared and further developed, and their value assessed including the validation of the methodologies for uncertainty propagation in HTGR modeling. The uncertainty propagation will be estimated through the whole simulation process on a unified benchmark framework to provide credible coupled code predictions with defensible uncertainty estimations of safety margins at the full core/system level. The proposed program will help to utilize the community of experts created during the previous IAEA and OECD HTGR-related activities and expand it by combining expertise in physics (neutronics and thermal-hydraulics) and in SA and UA. The CRP will allow not only comparison to and assessment of the current SA and UA methods on representative applications, but the program will also stimulate further development of efficient and powerful SA and UA methods suitable for complex coupled code simulations. The CRP will also help to formulate recommendations and guidelines on how to utilize advanced and optimized SA and UA methods in "best-estimate" reactor simulations in HTGR licensing practices.

The objective is to determine the uncertainty in HTGR calculations at all stages of coupled reactor physics/thermal-hydraulics and depletion calculations. To accomplish this objective, a benchmark platform for uncertainty analysis in best-estimate coupled code calculations for design and safety analysis of HTGRs will be defined and utilized. The full chain of uncertainty propagation from basic data, engineering uncertainties, across different scales (multi-scale), and physics phenomena (multi-physics) will be tested on a number of benchmark exercises with maximum utilization of the available experimental data, published benchmark results, and released design details. Two main HTGR types (prismatic and pebble-bed HTGRs) are selected based on previous benchmark experiences and available data.

The comparative analysis results of the completed OECD Pebble-Bed Modular Reactor (PBMR)-400 Coupled Code Benchmark [2,3] and CRP5 benchmark analysis related to the PBMR-400, Pebble-Bed Micro Model, Gas Turbine Modular Helium Reactor, HTR-10, and the ASTRA critical facility [6,7] have demonstrated the need of such an HTGR UAM program. Differences between the code-to-code comparisons but also the analysis of experiments showed large differences that could not be explained fully and that were often assigned to model variations or experimental uncertainties.

The effort to establish a methodology for very-high-temperature reactor (VHTR) uncertainty treatment is best suited within the framework of an international cooperation under the coordination of the IAEA. The effort will include careful interfacing with the OECD LWR UAM, as well as with international and national Generation IV VHTR activities.

1.2   Preparation Meetings for the CRP

The first consultancy meeting on this subject was held June 14–17, 2010, in Vienna, where participants from several member states presented their work in this area and expressed their interest in joining the proposed CRP. The broad scope of the CRP was also defined at this meeting. The second meeting was convened to coincide with the High-Temperature Reactor Technology 2010 Conference, which took place in Prague in October 2010, and took advantage of the presence of more experts in the field of HTGRs. The third and final consultancy meeting took place in Vienna, in the IAEA headquarters July 12–14, 2011. The meetings were also open to experts from IAEA member countries, which are in a position to provide a substantive contribution to this study.

1.3 Organization Arrangement for the CRP Benchmark Specification

The following organizational structure was accepted at the Second Research Coordination Meeting (RCM) on the Uncertainty Analysis in HTGR Modelling Physics, Thermal-Hydraulics, and Depletion Uncertainty Analysis that took place in December 2014 at the IAEA Headquarters in Vienna, Austria:

Working Groups Overall Coordinator: Kostadin Ivanov (Pennsylvania State University)

Scientific Secretary: Frederik Reitsma, IAEA

Pebble Bed Reactors Working Group – **Coordinator – Frederik Reitsma**

IAEA: Frederik Reitsma (Neutronics Track Leader)

INET: Li Fu (Thermal Fluids Track Leader)

INL: Gerhard Strydom (Fuel Physics Track Leader)

Pennsylvania State University: Kostadin Ivanov

North West University: Vishnu Naicker

Prismatic Reactors Working Group – **Coordinator – Gerhard Strydom**

Kurchatov: Victor Boyarinov (Neutronics Track Leader)

INL: Gerhard Strydom (Thermal-Fluids and Fuel Physics Track Leader)

Korea Atomic Energy Research Institute (KAERI): Jae Man Noh

Northwest University: Vishnu Naicker

This list and responsibilities will be updated as required and is dependent on the final list of participating countries and institutions in the CRP.

1.4 Scope and Technical Content of the Benchmark Problem

The scope of the benchmark is to establish a well-defined set of problems to compare methods and tools in core simulation and thermal-hydraulics analysis with a specific focus on uncertainty analysis and propagations. The uncertainty in the calculations during sensitivity and uncertainty analyses methods and their propagation in HTGR modeling will be compared. It is important to note that the primary focus of this benchmark, as opposed to the two OECD/NEA benchmarks on the PBMR-400 [2] and MHTGR-350 [5] designs, is not the comparison of the various code results, but the uncertainties in the reported output data. Although the participants' solution methodologies and flux, power, and temperature data are of interest, the main focus here is on the magnitude and behavior of the propagated uncertainties and sensitivities.

The benchmark will be executed in four phases, each containing several exercises to be performed. These phases are listed in Section 2. It starts with local stand-alone cell and lattice calculations in neutronics and thermal-hydraulics (Phase I), and then increases in scope to global stand-alone core level (Phase II) and global coupled exercises (Phase III). The exercises defined for Phase IV include feedback from the secondary system.

The calculations performed will be able to provide useful outcomes for core simulation and thermal-hydraulics analysis. Results would provide a quantitative assessment of the effect of propagated input uncertainties on defined figure of merit output uncertainties. Furthermore, the benchmark will provide important sources of uncertainties, including physical data, technological data, and model approximations.

2.   PHASE AND EXERCISE OVERVIEW

Separate specifications will be prepared for each phase to allow participation in the full phase or in only a subset of the exercises. Boundary conditions and necessary input information are provided for each phase so that it does not rely on the previous phase, although the results from a phase may be used to define or refine the input uncertainties of subsequent phases.

The intention is to follow the calculation scheme for prismatic HTGR design and safety analysis as far as possible. Due to limitations in many code systems, the exercise definitions—and therefore the proposed calculation scheme—are loosely based on the scheme used and established in the LWR power generation industry. This implies that the analyses are broken up into distinct steps such as cell calculations, assembly calculations and full core calculations (steady-state and time-dependent), and design and safety calculations.

2.1   Approach to Uncertainty Analysis

In principle, the sources of Input (I) uncertainties in computer code simulations are identified as:

- Uncertainties of input data

- Model limitations

- Approximations in the numerical solution

- Nodalization

- Homogenization approaches

- Imperfect knowledge of boundary and initial conditions.

For each exercise, it is important to identify which new input uncertainties are taken into account and which input uncertainties are propagated from the previous exercise. In the neutronics Phase I of the benchmark, the input uncertainties are specified as follows: best-estimate values for input parameters supplemented by the variance-covariance matrices (utilized for cross-section uncertainties) and for other input uncertainties—probability distribution functions and associated parameters.

Other important parameters to be defined are the Output (O) uncertainties and propagated Uncertainty parameters (U) for each exercise. This task is directly related to the objective of each exercise. The Output (O) uncertainties are defined for specified output parameters for each exercise to test (evaluate) the utilized uncertainty method. The propagated Uncertainty parameters (U) are output parameters selected to be propagated further through the follow-up exercises to calculate the overall resulting uncertainty. The aim is to propagate as many uncertainties as feasible and realistic to the subsequent coupled calculations.

2.2   The Phases and Exercises

The benchmark specification for Phase I require the modeling of local effects. It is divided into the following exercises.

2.2.1   Exercises I-1 and I-2: Local Neutronics

These exercises are focused on the derivation of the multi-group and few-group microscopic cross-section libraries. The objective is to address the uncertainties due to the basic nuclear data, as well as the impact of processing the nuclear and covariance data, selection of multi-group structure, and double heterogeneity or self-shielding treatment. The intention is to propagate the uncertainties in evaluated Nuclear Data Libraries (microscopic point-wise cross sections) into multi-group microscopic cross sections and to propagate the uncertainties from the multi-group microscopic cross sections into the few-group cross sections for use in Phase II. Two exercises are defined t

Exercise I-1 (I-1a, I-1b) – Cell Physics: Derivation of the multi-group microscopic cross-section libraries.

Two basic unit cells are defined for Exercise 1 based on the MHTGR-350 design parameters. Two sub-cases are included: Exercise I-1a specifies a homogeneous fuel region of homogenized triple-coated isotropic particle (TRISO) fuel particles and matrix graphite, whereas Exercise I-1b requires the explicit modeling of the tristructural-isotropic (TRISO) fuel particles to investigate their self-shielding effect on the multi-group microscopic cross-sections.

Exercise 1-2 (I-2a, I-2b, I-2c) – Lattice Physics: Derivation of the few-group macroscopic cross-section libraries

Exercise I-2a requires a lattice calculation to be performed on a single fuel block at hot full power (HFP) conditions, while Exercise I-2b specifies the same problem at 100 MWd/kg-U burnup. Exercise I-2c adds the spectral effects of the neighboring domain by performing a lattice calculation on a supercell (or mini-core), which consists of a fresh fuel block surrounded by a mixture of depleted and fresh fuel on one side and graphite reflector blocks on the other side. This calculation is also performed at HFP conditions.

2.2.2   Exercises I-3 and I-4: Local Thermal-Hydraulic coupling

These exercises are focused on the localized stand-alone fuel thermal response. The aim of the stand-alone thermal unit cell calculations is to isolate the effect of material and boundary input uncertainties on very simplified problems before the same input variations are applied to complex core problems (Phases II–IV). The figures of merit for both exercises are the variation in the unit cell temperature profiles due to input uncertainty variations in the material properties and boundary conditions. No output parameters will be propagated into subsequent exercises or phases, but the same material input uncertainties (also called manufacturer uncertainties) will be specified in the subsequent phases.

Exercise I-3 (I-3a, I-3b): Stand-alone thermal-hydraulics (normal operation)

Exercise I-3 requires a steady-state solution for a single fuel compact and coolant channel unit cell with a fixed bulk coolant temperature. Two sub-cases similar to Exercise I-1 are again defined here, taking into account the explicit modeling of heat transfer from the TRISO fuel particles to the matrix graphite.

Exercise I-4 (I-4a, I-4b): Stand-alone thermal-hydraulics (power excursion transient)

Exercises I-4a and I-4b use the same unit cell definition as described for Exercise I-3, but a time-dependent power excursion is prescribed, as opposed to a constant steady state power. The two case variations here are designed to study the effect of additional uncertainties in the explicit modeling of the $UC_{0.5}O_{1.5}$ TRISO kernels (e.g., variations in the SiC thickness, density, and conductivity).

2.2.3   Phase II: Global Standalone Modeling

Exercise II-1a: Core physics: Criticality (steady-state) stand-alone neutronics calculations

A full-core steady-state neutronics calculation is to be performed using the given fuel number densities and core temperature distributions.

Exercise II-1b: Core physics: Stand-alone kinetics without feedback

This exercise involves a full-core calculation with reactivity being added and then returned to normal but without any temperature feedback. The reactivity induced transient is defined as control rod movement at normal or even slower speed to ensure that the delayed neutrons play a role (no prompt critical effects). The uncertainties in the kinetic parameters are added in this case.

Exercise II-2a: Stand-alone thermal-hydraulics focused on core thermal-hydraulic modeling (normal operation)

The conditions at normal operation are considered with only the reactor core modeled and with boundary conditions defined for the inlet coolant temperature and pressure and the vessel defined with a constant temperature boundary condition. The reactor power distribution is also specified. Variation in bypass flows and pebble packing fractions are some of the uncertainties to be taken into account.

Exercise II-2b: Stand-alone thermal-hydraulics focused on core thermal-hydraulic modeling (depressurized loss of forced cooling transient)

A depressurized loss of forced cooling calculation from full-power conditions is performed. The uncertainties in the steady-state power profile and temperatures from Exercises II-1a and II-2a are input to this calculation. The decay heat uncertainties also need to be addressed.

2.2.4 Phase III: Design Calculations

Exercise III-1: Coupled steady state

This is the first exercise that requires a coupled calculation focused on the steady-state full-power neutronics/thermal-hydraulics core performance. Many of the uncertainties determined in the previous stand-alone cases will be propagated.

Exercise III-2: Coupled depletion

The depletion is added to the full core coupled neutronics/thermal-hydraulics core calculation, and an equilibrium cycle is to be calculated. Alternatively, a simplified depletion case with given power history may be evaluated.

2.2.5 Phase IV: Safety Calculations

Exercise IV-1: Coupled core transient

The coupled core transient with full thermal feedback will be a reactivity-induced power excursion due to control rod withdrawal. The feedback effect from the rest of the power conversion unit is to be kept constant or described by a well-defined function. Thus, the focus is on the core response only.

Exercise IV-2: Coupled system transient

The transient of interest is the change in helium inlet coolant temperature with the associated feedback on neutronics, which focuses on the coupled core/thermal-hydraulic system transient performance.

Volume I of the CRP on HTGR UAM (this document) contains the specification for the exercises of Phase I, as well as the unit cell and lattice specifications for the Very-High-Temperature Reactor Critical (VHTRC) experimental benchmark. The definitions of the neutronics-only Exercises I-1 and I-2 are provided in Section 3 and Section 4, respectively. This is followed by the specifications for the stand-alone thermal-hydraulic Exercises I-3 and I-4 in Section 5. A summary is provided in Section 6. The appendices contain information on the material properties and manufacturing uncertainties, an output template example, and the major changes made during this revision.

3.   EXERCISE I-1: LOCAL NEUTRONICS – CELL PHYSICS

This exercise is identical in scope and objectives to the Exercise I-1 (Cell Physics) of the OECD LWR uncertainty benchmark [4], and most of the details on the use of covariance data are directly applicable. Therefore, sections from that document are reproduced here. In the typical LWR lattice approach, this exercise is focused on the derivation of the multi-group microscopic cross-section libraries, but in practice this scheme of cell-lattice-core cross-section generation is not used for prismatic HTGR

designs, where the cell physics step is skipped and single blocks, or larger regions of blocks, are used to generate multi-group cross sections.

The objective of this exercise is to address the uncertainties due to the basic nuclear data, as well as the impact of processing the nuclear and covariance data, selection of multi-group structure, and double heterogeneity or self-shielding treatment. It is possible to propagate these uncertainties from Phase I to Phase II (i.e., the output uncertainties of Exercise I-1 can be used as input uncertainties in Exercise I-2). Alternatively, participants can decide to directly perform all cell and lattice calculations in a fine group structure (e.g., 238 groups) and propagate the single-block or supercell uncertainties directly to Phase II through the few-group cross-section libraries. The uncertainties can be propagated using a broader group structure, if desired. For this benchmark, the uncertainty propagation through the use of cell-to-lattice cross-section libraries from Exercise 1 to Exercise 2 is not required. Nevertheless, participants are encouraged to report their uncertainty analysis results for Exercise 1 as a measure of the methodology applied to simple problems.

3.1   Uncertainties in Nuclear Data

The evaluation of nuclear data induced uncertainty is possible by the use of nuclear data covariance information. To evaluate the importance of cross-section uncertainties in prismatic HTGRs, the availability of measured covariance data is important for all relevant nuclides (actinides, fission products, absorbers, structural materials, etc.) present in the reactor core and reflector regions, covering the entire energy range of interest (from 0 to 10 MeV), and for all relevant reaction cross-section types.

In Chapter 2 of Reference 4, a detailed description of the status of nuclear covariance information is provided. The covariance data in the major data files are scarce in terms of materials (including actinides) and types of covariance matrices available. They contain uncertainty information only for few isotopes and reactions and usually for different number and different isotopes in different files. For isotopes not included, usually their covariance is assumed to be zero, which will result in the underestimation of core parameters uncertainties. The conclusion reached in Reference 4 is that the status of available covariance data in the major nuclear data libraries (NDLs) is such that it cannot support the objectives of the OECD LWR UAM benchmark. The same is thus assumed to be true in this exercise. The development of nuclear data covariance files is in progress in the major NDLs and could be available for future application.

The participants can use any of the major NDLs such as Evaluated Nuclear Data Files (ENDFs), Joint European Fission and Fusion Files, or Japanese Evaluated Nuclear Data Library. As already mentioned, the available covariance data on these libraries are limited. The most complete covariance data are currently available for the latest version of the Oak Ridge National Laboratory (ORNL) SCALE code package in the form of several evaluations of multi-group uncertainty libraries. The SCALE code package is a collection of all covariance data that were produced over the last few decades and critically reviewed for the most important nuclides. The package is organized into 44 groups and can be expanded or reduced to the participants' multi-group structures.

Prior to using the covariance information in applications, a processing method/code must be used to convert the energy-dependent covariance information to a multi-group format. Within the framework of Exercise I-1, the participants can use/develop their own processing methods or utilize available tools/codes at NEA/OECD and Radiation Safety Information Computational Center/ORNL to process the cross-section data and associated covariance data (group-wise covariance matrices) for the multi-group libraries utilized as input in their lattice physics codes.

3.2   MHTGR-350

3.2.1   Exercise I-1a to Exercise I-1d: Fuel Compact Unit Cell Calculations

One of the objectives of the benchmark is to provide recommendations for physical and numerical models suitable for reactor physics and uncertainty analysis. For that purpose, participants will be

requested to provide information about the models they use. In the absence of cell-level experimental data, continuous-energy Monte Carlo (Serpent) "reference" solutions with sufficient statistics to ensure k_{inf} and fission source convergence were created by the INL team for Exercise 1a-2c. The set of reference calculations for all Phase I exercises were reported at the 2014 RCM in Vienna and summarized in INL/EXT-14-32944 [8]. The statistical uncertainties in the reference calculations were also evaluated and reported by the benchmark team, as well as comparison calculations with the ENDF-VI Versions 0 and 1 libraries to assess the effect of evaluated NDLs on the problem set. *Note that INL/EXT-14-32944 will be updated in 2015, since the reference results were created using an older version of this document.*

A hexagonal representative two-dimensional "unit cell" for the MHTGR-350 fuel is shown Figure 1 consisting of the $UC_{0.5}O_{1.5}$ fuel compact, a small gap, and the surrounding block graphite. The hexagonal cell definition shown in Figure 1 is consistent with the LWR UAM cell definitions for the VVER design [4]. This unit cell is derived from the larger fuel block hexagonal geometry, as shown in Figure 4, where each of the blue helium coolant channels remove the heat generated by two of the yellow fuel compacts. The only difference between Exercise I-1a and Exercise I-1b is the modeling of the fuel zone: Exercise I-1a specifies a homogeneous fuel region of "smeared-out" TRISO fuel particles and matrix graphite, whereas Exercise I-1b requires the explicit modeling of the TRISO fuel particles to investigate their self-shielding effect on the multi-group microscopic cross sections.

At the RCM in 2014, some participants suggested that the homogenous cell problem (Exercise 1a) is unrealistic because it ignores the well-known double heterogeneous impact, and that this variant should be treated as optional. As stated before, no data will be propagated in any case from Exercise 1 to the subsequent exercises, so both variants are in essence "test" exercises to compare participants' methods and initial results. As the problem definitions are almost identical, the simulation burden of Exercise 1a is not prohibitive, and Exercise I-1a is still currently still part of the specification set.

A second issue raised at the second RCM was the harder spectrum obtained using the simple cell definition in Figure 1, as reported in Reference 8, because the moderator-to-fuel ratio of the hexagonal unit cell is approximately 0.5 of the block-moderation ratio. This could be "corrected" by increasing the graphite density or by reducing the fuel inventory to match the block average value. However, it was decided to include a triangular geometry variant of the unit cell geometry, as shown in Figure 2 for Exercise I-1c (homogeneous case) and Exercise I-1d (heterogeneous case). The dimensions of the triangular cell are provided in Figure 3. It should be noted that the MHTGR-350 design contains 102 large and six small coolant holes per a standard fuel element, but for this exercise, only the large coolant hole geometry will be included in Exercise I-1c/d, i.e., r = 0.794 cm. (Both hole types are included in Exercise I-2.) Because both unit cells are based on the same fuel block data, the geometry and number density data shown in Table 3, Table 4, and Table 5 are valid for both sets of data.

At this point, both cell geometries are included in this revision of the specifications. Participants are encouraged to determine whether the differences in the figures of merit (e.g., k_∞ uncertainty estimates, not k_∞ itself) warrant the inclusion of both hexagonal and triangular geometries in future revisions of this specification. (An investigation performed at INL showed that the triangular cell produced a softer spectrum, but also that it was still far away from the supercell [Exercise I-2c] reference spectrum. These findings will be included in the update of INL/EXT-14-32944 [8].)

A reflective boundary condition is specified, because most of the fuel compacts are surrounded by identical unit cells. (The exception to this assumption is addressed in the next lattice level exercise.) The unit cell number densities are defined for two subcases: a xenon-free cold zero power (CZP) and a xenon-free HFP core state. The temperature points of 293 K and 1,200 K were selected to coincide with the ENDF-VI library points. As stated before, creation of Exercise 1 multi-group cross-section libraries is not required for use in the lattice (Exercise I-2) calculations. However, these simplified "unit cell" cases can still be used to identify the major contributors to the multi-group cross-section uncertainties with a reduced simulation burden, and explore the use of various tools.
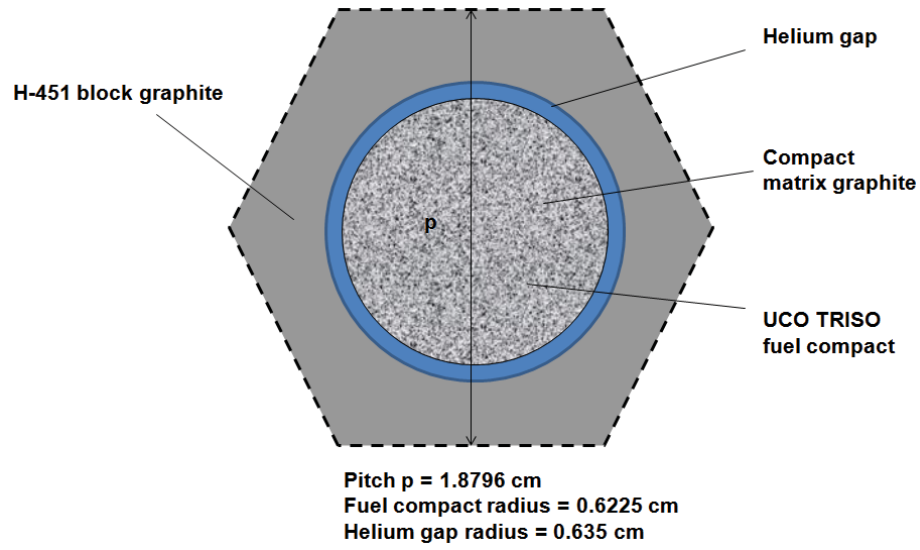
Figure 1. Hexagonal MHTGR unit cell for Exercises I-1a and I-1b.
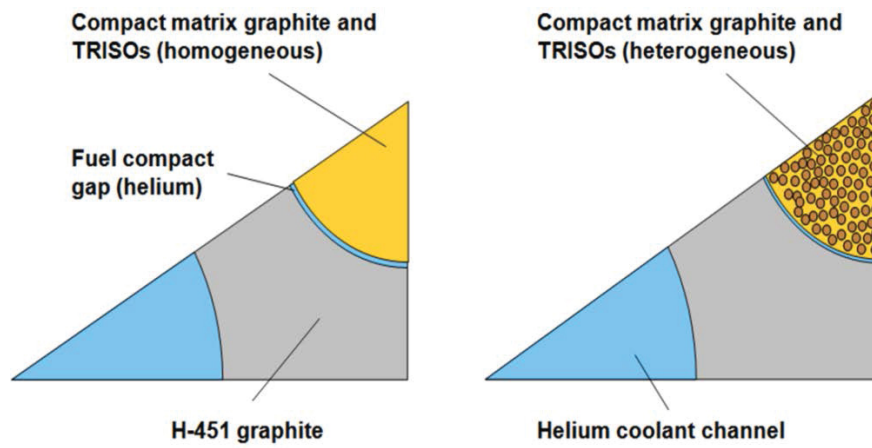
Figure 2. Triangular MHTGR unit cell for Exercises I-1c (left) and I-1d (right).
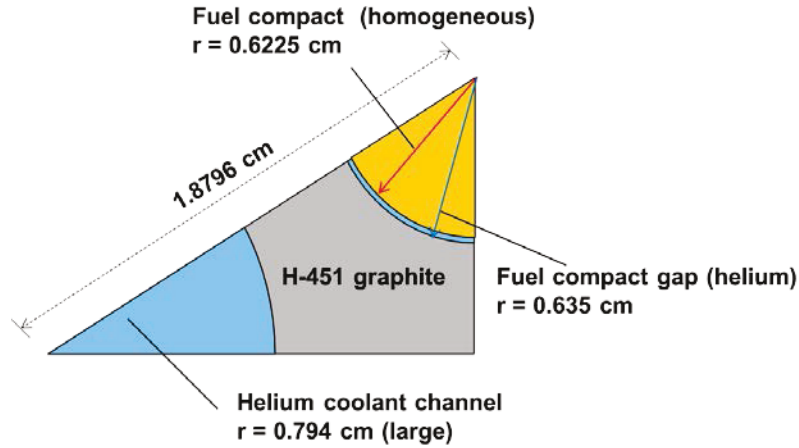
Figure 3. MHTGR-350 triangular unit cell dimensions.

The data for all Exercise I-1 cases are specified in Table 1 through Table 5. This "nominal" or best–estimate information is repeated in Appendix D, together with the material and manufacturing uncertainty information. The $UC_{0.5}O_{1.5}$ fuel kernels are contained in TRISO fuel particles that have an outer radius of 427.5 μm and a ^{235}U enrichment of 15.5 wt%. The packing fraction of the TRISO fuel particles is 35% in the fuel compacts with the remaining volume being composed of matrix graphite.

Table 1. Operating conditions for Exercise I-1.

Parameter/Reactor Condition	CZP	HFP
Temperature of all material in fuel compact (K)	293	1,200
Temperature of helium in gap (K)	293	1,200
Temperature of H-451 block graphite	293	1,200
Reactor power (MWt) (if required)	0.35	350

Table 2. Dimensions for Exercise I-1a and I-1c.

Parameter	Dimension (cm)
Fuel compact outer radius	0.6225
Fuel/helium gap outer radius	0.6350
Unit cell pitch	1.8796
Fuel compact height	4.9280

Table 3. Dimensions for Exercise I-1b and I-1d.

Parameter		Dimension (cm)
TRISO Fuel Particle	$UC_{0.5}O_{1.5}$ kernel radius	2.125E-02
	Porous carbon buffer layer outer radius	3.125E-02
	Inner PyC outer radius	3.525E-02
	SiC outer radius	3.875E-02
	Outer PyC outer radius	4.275E-02
Average TRISO packing fraction		0.35
Fuel compact outer radius		0.6225

10

Fuel/helium gap outer radius	0.6350
Large helium coolant channel radius [a]	0.7940
Unit cell pitch	1.8796
Fuel compact height	4.9280
a. The standard fuel block contains much more large (102) than small (6) coolant channels. For Exercise I-1c/d, only the large coolant channel case is selected.	

Table 4. Number Densities for Exercise I-1a and I-1c.

Nuclide		**Number Density (atoms/b·cm)**
Homogenized fuel region	^{235}U	1.5765E-04
	^{238}U	8.4864E-04
	^{16}O	1.5094E-03
	Graphite[a]	6.9958E-02
	^{28}Si	2.8457E-03
	^{29}Si	1.4456E-04
	^{30}Si	9.5408E-05
Coolant channel	^{4}He	2.4600E-05
H-451 block graphite	Graphite	9.2756E-02
a. Graphite is defined here as natural carbon including thermal scattering data for graphite. In the SCALE code, this is C-graphite; in Serpent/MCNP, this is natural carbon with the additional thermal scattering data applied. This definition is applied for all neutronics problems in this benchmark. A sensitivity study performed at INL showed minor differences if various mixtures of C-nat and C-graphite are used [8], and it has been decided at the 2nd RCM to consistently use C-graphite for all carbon in this specification.		

Table 5. Number densities for Exercises I-1b and I-1d.

Number Densities		Nuclide	ND (at/b-cm)
TRISO Fuel Particle	Kernel	^{235}U	3.6676E-03
		^{238}U	1.9742E-02
		^{16}O	3.5114E-02
		Graphite	1.1705E-02
	Porous Carbon	Graphite	5.2646E-02
	IPyC	Graphite	9.5263E-02
	SiC	^{28}Si	4.4159E-02
		^{29}Si	2.2433E-03
		^{30}Si	1.4805E-03
		Graphite	4.7883E-02
	OPyC	Graphite	9.5263E-02
Compact matrix		Graphite	7.2701E-02
Coolant channels		^{4}He	2.4600E-05
H-451 block graphite		Graphite	9.2756E-02

3.2.2   Input Uncertainty Parameters

The input uncertainties arise from:

- Multi-group cross-section uncertainties (multi-group cross-section covariance matrix)

- Fuel/assembly manufacturing uncertainties such as unit cell dimensions and nuclide densities (see Appendix C, Table C-1 and Table C-2 for Exercise I-1a-d)

- Uncertainties associated with methods and modeling approximations utilized in lattice physics codes, including the selection of the multi-group structure and treatment of the double heterogeneity or self-shielding.

Participants can use their own lattice physics codes in conjunction with their own UA and SA tools for the purposes of this exercise. *Only the first two input uncertainties will be included for assessment in this HTGR UAM, since the quantification of method/model approximations is code-dependent and beyond the scope of this benchmark (see Section 4.1 as well).*

3.2.3   Output Parameters to be Compared

The required output for Exercise I-1 is described in Appendix C. The appendix includes examples of completed output template pages, as well as the Excel template files. The Excel templates can either be uploaded from Appendix B or requested via e-mail from the IAEA CRP coordinator.

3.2.4   Propagated Parameters

A multi-group cross-section variance (covariance matrix) can in principle be used to create multi-group cross-section libraries for use in the lattice calculation ExerciseI-2, but it has been decided at the 2nd RCM to make this step optional (see Appendix E). Participants can utilize their own sensitivity/uncertainty tools to calculate quantities of interest, or participants can use the tools available at NEA/OECD (e.g., SUSD3D [9]) and ORNL (e.g., TSUNAMI [10]).

4.   EXERCISE I-2: LOCAL NEUTRONICS – LATTICE PHYSICS

4.1   Sources of Input Uncertainties

Exercise I-2 includes the propagation of input uncertainties through lattice physics calculations to output uncertainties in evaluated lattice-averaged parameters. Examples of these parameters could be few-group homogenized parameters such as cross-sections, assembly discontinuity factors, form functions, and k_∞. The input uncertainties arise from:

- Multi-group cross-section uncertainties (multi-group cross-section covariance matrix)

- Uncertainties associated with methods and modeling approximations utilized in lattice physics codes

- Fuel/assembly manufacturing uncertainties.

Participants can use/select their own lattice physics codes in conjunction with their own UA and SA tools for the purposes of this exercise. In the current LWR standard calculation scheme, the lattice physics calculations for generation of few-group cross sections usually apply the following scheme:

1. Pin cell homogenization

2. Energy group condensation

3. Assembly homogenization in a single-assembly environment.

The spectral effects of neighboring blocks play an important role in HTGR physics, and it has been shown that the utilization of a single block with infinite reflective boundary conditions to create few-group cross sections is not acceptable for high-fidelity core solutions [11]. A more representative spectral environment can be obtained by designing appropriate two-dimensional mini-core test problems (also called supercells or color sets), in addition to two-dimensional single-assembly models with reflective boundary conditions. The latter are the base models for cross-section generation with the exception of reflector cross sections, which are usually generated in one-dimensional color sets. For this reason, an example of a two-dimensional supercell (or mini-core) test problem is defined by the benchmark team for Exercise I-2c, in addition to the single-block lattice Exercise I-2a.

4.1.1   Multi-Group Cross-Section Uncertainties

In the current established calculation scheme for LWR design and safety analysis, multi-group microscopic cross-section libraries are an input to lattice physics calculations. A similar methodology can be followed for prismatic HTGR designs, although special attention is required for the definition of a lattice cell in these thermal graphite-moderated systems. Because the propagation of uncertainties from the cell (ExerciseI-1) to the lattice phase is not required, participants can directly calculate a Phase II few-group library using a sufficiently accurate fine-group library as input for Exercise I-2, together with the cross-section covariance data. All cross-section uncertainties are assumed to follow normal Gaussian distributions, and only the first and second moments of the uncertainty distributions (i.e., the means and co-variances) are to be propagated through the calculations.

4.1.2   Uncertainties Associated with Methods and Modeling Approximations

The second source of input uncertainties in Exercise I-2 are additional uncertainties added during the multi-group cross-section generation process. Methodological uncertainties, which are associated with methods and modeling approximations utilized in lattice physics codes, should be assessed by participants using the specific tools as a separate effort, but a comparison of this class of uncertainties is beyond the scope of the benchmark. For example, various transport methods have been utilized in lattice physics codes—the Collision Probabilities Method, the Method of Characteristics, S_n, P_n, etc., each with their specific approximations and uncertainties. The evaluation of other nodal homogenized parameter

uncertainties (e.g., Assembly Discontinuity Factors and Form Functions) is likewise left up to participants to report on in separate technical reports (i.e., it will not form part of the compared data set at this point).

However, the participants are responsible to perform spatial and angular discretization convergence studies with their lattice physics codes to remove the uncertainties associated with numerical approximations (numerical method uncertainties).

4.1.3 Manufacturing Uncertainties

The third source of input uncertainties is fuel/assembly manufacturing uncertainties such as enrichment, pellet density, cladding dimensions, burnable poison (BP) concentration, and assembly geometry. Assignment of uncertainty measures in the form of probability distribution functions are provided in Appendix C, Table C-3 and Table C-4. The same input uncertainties as defined for Exercise I-1 should be applied to Exercise I-2. This information is of secondary importance (the main focus is on cross-section uncertainties), but participants are encouraged to submit an assessment of these uncertainties, either in combination with the cross-section data uncertainties or as a stand-alone uncertainty quantification.

4.1.4 Propagation of Input Uncertainties

Within the framework of Exercise I-2 the above-described input uncertainties can be propagated through lattice physics calculations to the few-group lattice-averaged (homogenized assembly/node) parameters for use in the Phase II core solvers. Participants are requested to focus mostly on cross-section uncertainty propagation and, if their capabilities and resources allow, to also propagate in parallel the manufacturing uncertainties in Exercise I-2. Participants in the HTGR UAM are advised to track the ongoing progress reported by the OECD/NEA LWR UAM benchmark teams and to obtain practical examples of the uncertainty quantification process discussed here.

4.2 Requested Output

The required output for Exercises I-2a, I-2b and I-2c are described in Appendix B. The appendix includes examples of completed output template pages, as well as the Excel template files. The Excel templates can either be uploaded from Appendix B or be requested via e-mail from the IAEA CRP coordinator.

4.3 Propagated Parameters to Phase II

It is expected that most participants will follow a statistical approach (e.g., XSUSA/SAMPLER) to generate perturbed few-group libraries for use in the Phase II core solvers. It is already known that the traditional LWR two-group approach results in poor core solutions for HTGR systems [11]. Several few-group HTGR structures have been investigated before, e.g., General Atomics validated a nine-group structure from integral Fort St. Vrain measurements; researchers at KAERI suggested a 10-group structure [12]; and the OECD MHTGR-350 benchmark uses a 26-group structure to mitigate spectral, BP, and control rod effects [4]. At the 2nd RCM, it was decided to compare the Phase II core solutions using the 26-group structure, but participants are also encouraged to compare various few-group energy structures in separate side studies. More details will be provided in the specifications for Phase II.

4.4 MHTGR-350

4.4.1 Exercise I-2a and Exercise I-2b: Fresh and Depleted Single-Fuel Block Lattice Calculations

The geometry and isotopic data for the simplified single MHTGR-350 hexagonal fuel blocks are shown in Figure 4 and specified in Table 6, Table 7 (Exercise I-2a), and Table 8 (Exercise I-2b). Two simplifications have been made to the original MHTGR-350 fuel specification:

- The fuel handling hole and positions for dowels are omitted for simplicity and filled with H-451 block graphite.

- Gaps up to 5 mm are required in the MHTGR-350 design between the fuel and reflector blocks to allow dimensional changes as a function of temperature and fluence. In the core thermal-hydraulic specifications of Phase II, a 2 mm gap will be included between the blocks. This 2 mm gap is neglected in the Phase I Exercise 2 calculations, i.e., it is assumed the blocks have no gaps between them, and the block flat-to-flat (or mid-point to mid-point) dimension is 36 cm. This approximation is acceptable for the neutronics calculations, but the gap plays an important role in calculation the bypass helium flow.

The <u>fresh</u> fuel block defined for Exercise I-2a (Figure 4) includes six lumped burnable poison (LBP) compacts in the six corners of the block. For the <u>depleted</u> fuel block defined for Exercise I-2b (also Figure 4), it is assumed that all LBPs have been fully depleted and are replaced by H-451 block graphite. The full set of 279 nuclide densities for the depleted fuel kernels is provided in a text file embedded here as Figure 5. The nuclide densities were obtained by performing a Serpent depletion calculation of the Exercise I-2a fresh block *without BP* up to 100 MWd/kg-U. This decision is based on the results shown in the INL Phase I report [8] that depletion performed using the relatively hard spectrum of a single fresh block with LBPs led to significant errors. A constant power density of 0.1 kW/g initial uranium and no downtime was assumed. These assumptions were discussed and accepted at the 2nd RCM.

Both of these exercises require treatment of the double heterogeneity effects, i.e., the self-shielding that occurs both within the fuel and LBP compacts, as well as the effect of multiple compacts present in a single block. Note that the LBP compact itself consists of a several thousand coated particles of B4C with buffer and PyC coating layers, as indicated in Table 6.

It should also be noted that the block "edge" region shown in Figure 4 is not accurately represented (i.e., it is not exactly one-half of a hexagonal unit cell). Participants should not use this figure to develop their models; instead, participants should use the data in Table 6 and cross-check their calculations with the data included in Appendix D.
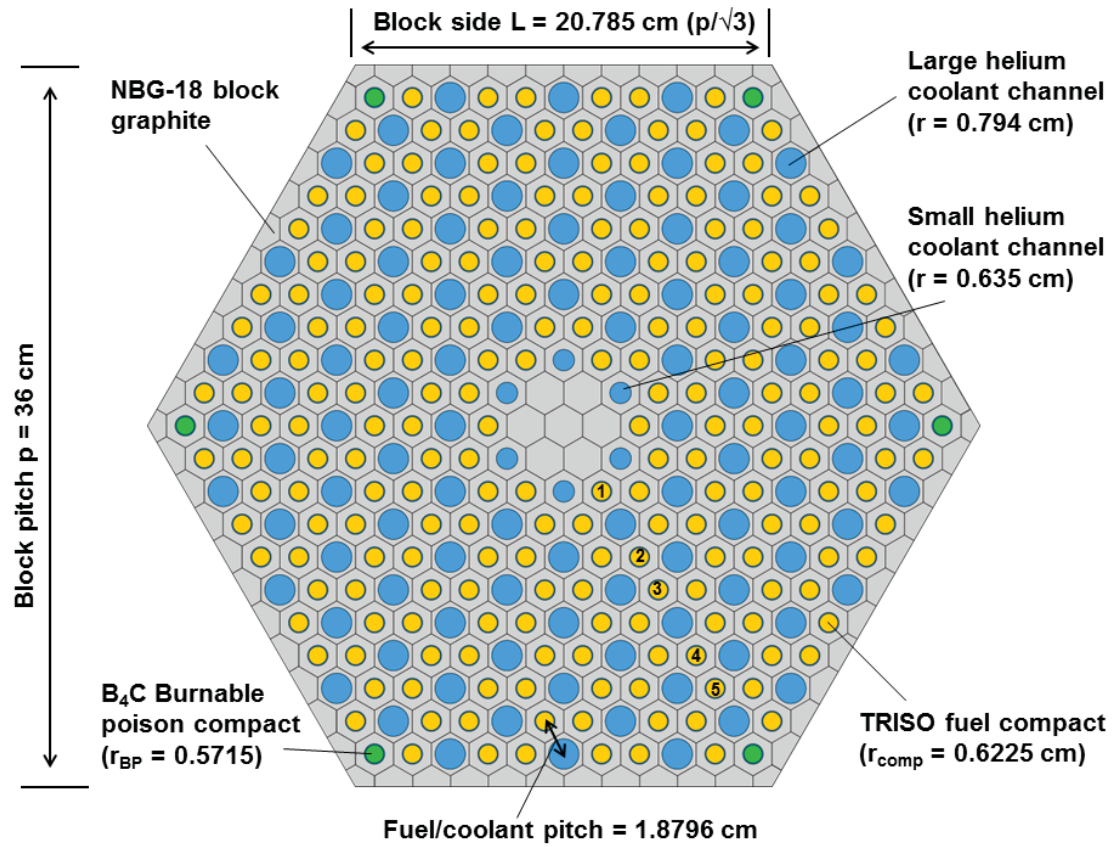
Figure 4. MHTGR-350 lattice cell for Exercise I-2 (single block).

Table 6. TRISO and block dimensions for Exercise I-2.

Parameter		5. Dimension	6. Units
TRISO fuel particle	$UC_{0.5}O_{1.5}$ kernel radius	2.125E-02	cm
	Porous carbon buffer outer radius	3.125E-02	cm
	IPyC OR	3.525E-02	cm
	SiC OR	3.875E-02	cm
	OPyC OR	4.275E-02	cm
TRISO packing fraction		0.35	—
Fuel compact radius		0.6225	cm
Gap radius		0.6350	cm
Number of fuel compacts per block		210	—
LBP particle	Kernel radius	0.0100	cm
	Porous carbon buffer outer radius	0.0118	cm
	PyC outer radius	0.0141	cm
BP particle packing fraction		0.1090	
BP compact radius		0.5715	cm
Large coolant channel radius		0.7940	cm
Number of large coolant holes		102	—
Small coolant channel radius		0.6350	cm
Number of small coolant holes		6	—
Pin pitch		1.8796	cm
Block flat-to-flat width		36.0	cm
Block (compact) height		4.9280	cm

Table 7. Number densities for the fresh fuel block (Exercise I-2a).

Number Densities		7. Nuclide	8. N (at/b-cm)
TRISO fuel particle	$UC_{0.5}O_{1.5}$ kernel	^{235}U	3.6676E-03
		^{238}U	1.9742E-02
		^{16}O	3.5114E-02
		Graphite	1.1705E-02
	Porous carbon	Graphite	5.2646E-02
	IPyC	Graphite	9.5263E-02
	SiC	^{28}Si	4.4159E-02
		^{29}Si	2.2433E-03
		^{30}Si	1.4805E-03
		Graphite	4.7883E-02
	OPyC	Graphite	9.5263E-02
BP particle	Kernel	^{10}B	2.1400E-02
		^{11}B	8.6300E-02
		Graphite	2.6900E-02
	Buffer	Graphite	5.0200E-02
	PyC	Graphite	9.3800E-02
Fuel compact matrix		Graphite	7.2701E-02
BP compact matrix		Graphite	7.2701E-02
Coolant channels		^{4}He	2.4600E-05
H-451 block graphite		Graphite	9.2756E-02

Table 8. Number densities for the burned fuel block (Exercise I-2b).

Number Densities		Nuclide	N (at/b-cm)
TRISO fuel particle	$UC_{0.5}O_{1.5}$ Kernel	See data file (Figure 5)	See data file (Figure 5)
	Porous Carbon	Graphite	5.2646E-02
	IPyC	Graphite	9.5263E-02
	SiC	^{28}Si	4.4159E-02
		^{29}Si	2.2433E-03
		^{30}Si	1.4805E-03
		Graphite	4.7883E-02
	OPyC	Graphite	9.5263E-02
Fuel compact matrix		Graphite	7.2701E-02
BP compact matrix		Graphite	7.2701E-02
Coolant channels		^{4}He	2.4600E-05
H-451 block graphite		Graphite	9.2756E-02

ND_ExI_2b.dat

Figure 5. UC$_{0.5}$O$_{1.5}$ fuel kernel nuclide densities for the depleted fuel block (Exercise I-2b).

Only HFP conditions are considered for these two exercises, as shown in Table 9.

Table 9. HFP operating conditions for Exercise I-2a/b.

Parameter/Reactor Condition	HFP
Temperature of all materials in fuel compact (K)	1,200
Temperature of helium in gap (K)	1,200
Temperature of H-451 block graphite (K)	1,200
Temperature of all materials in BP compact (K)	1,200
Reactor power (MWt)	350

8.1.1   Exercise I-2c: Super-Cell (Mini-Core) Lattice Calculation

The use of reflective boundary conditions for reflector blocks next to the inner or outer reflectors leads to significant spectral variances, because these blocks are not surrounded by an infinite lattice of fuel blocks [11]. To investigate the effect of neighboring blocks on a typical lattice calculation, an example of a supercell or mini-core has been defined, as presented in Figure 6. In this example, Block 26 is surrounded by reflector blocks on the right and top boundaries, and by one fresh and two depleted fuel blocks on the left and lower boundaries. The blocks containing fuel are homogenized using the relative contributions of two depleted fuel blocks and one fresh fuel block, as shown in Figure 7. Only the central fresh fuel block is required to be modeled in its heterogeneous detail (LBP and TRISO compacts). This assumption relaxes the significant memory and computational resources required to model this supercell in full detail. Only the HFP conditions are required to be calculated (Table 10).

Table 10. HFP operating conditions for Exercise I-2c.

Block	Parameter/Reactor Condition	HFP
Fresh fuel block	Temperature of all materials in fuel compact (K)	1,200
	Temperature of helium in gap (K)	1,200
	Temperature of H-451 block graphite	1,200
	Temperature of all materials in BP compact (K)	1,200
Temperature of homogenized depleted fuel block (K)		1,200
Temperature of H-451 graphite reflector block (K)		1,200
Reactor power (MW$_t$)		350

Several supercells can be constructed from the MTHTGR-350 core loading; the example included here represents blocks located in the outer fuel ring next to the outer reflector. The spectral environment for Block 17, for example, would be significantly harder, since it is surrounded by fuel elements only. In a more accurate lattice calculation, few-group cross sections produced by several configurations of these supercells could be used in the core calculations. For this CRP, only the one example is included, as an

19

effort to quantify the uncertainties that arise from using the classic single-block approach versus the supercell or mini-core approach. A separate study is currently under way at INL to assess the differences between several representative supercell configurations.
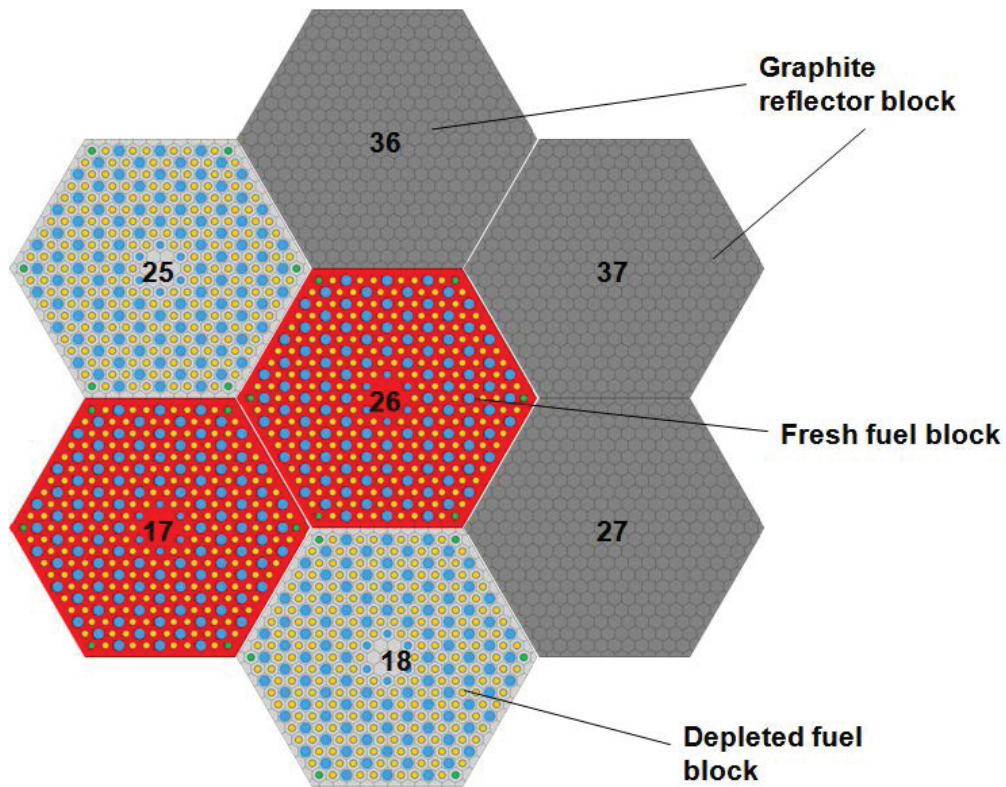
Figure 6. MHTGR-350 supercell centered at Block 26.
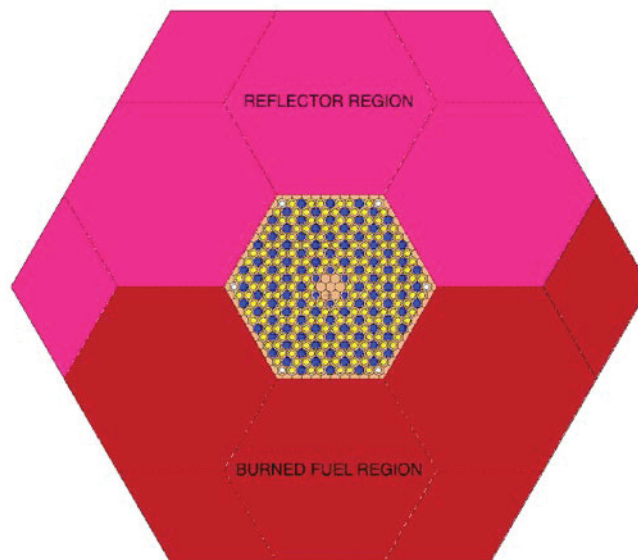
Figure 7. Simplified (rotated) representation of the Exercise I-2c supercell. The "burned" region consists of a homogenous mixture of two depleted blocks and one fresh fuel block.

The calculation will be performed on a supercell arrangement with dimensions and number density data identical to those given in Table 6 and Table 7 for the fresh fuel block. The only additional data element is the supercell flat-to-flat width of 108 cm (3 × 36 cm). The number densities for the reflector region are given in Table 11. A trace amount of neutron absorber impurities has been added to the reflector graphite specification, lumped into a ^{10}B equivalent boron content. It is assumed that these impurities do not deplete over time.

Table 11. Number densities for the reflector regions.

Number Densities	Nuclide	N (at/b-cm)
9. H-451 block graphite (reflector block)[a]	Graphite	9.2756E-02
	^{10}B[b]	2.7600E-08
a. In the actual MHTGR-350 design, different graphite grades were used for the reflector and fuel blocks. For the sake of simplicity, tt is assumed to be identical in this specification.		
b. The lumped impurities parameters equivalent boron content is specified here as ^{10}B.		

In order to reduce the amount of required calculation memory, it was accepted at the 2nd RCM (see Appendix E) that the full Serpent nuclide list obtained in Exercise I-2b be reduced to a smaller number of important nuclides. For this revision of the specifications, it was decided to utilize the standard 94 nuclides included in the SCALE/TRITON sequence as option "addnux=2". (For more detail, see the SCALE 6.1 User Manual, Table T1.3.4.) A test at INL revealed differences of several hundred per cent mille between the 94 nuclide set and a smaller set of 64 nuclides, included in TRITON as option "addnux=-2". It was therefore decided to perform the supercell calculation using 94 nuclides instead of the full Serpent list of 285 nuclides. This reduced set of 94 depleted number densities is provided in the text file embedded here as Figure 8. Note that this set already includes the homogenized volume ratios of one fresh and two burned fuel blocks.

ND_ExI_2c.dat

Figure 8. Number densities for the homogenized depleted fuel region (Exercise I-2c).

9.1   Exercise I-2 Validation Exercise: The VHTRC Experiment

There is a significant lack of validation data for prismatic HTGR designs, especially data sets where information on experimental and material uncertainties are included. For the validation exercise of Phase I, the cell and lattice phases (Exercises I-1 and I-2) are represented by the VHTRC assembly [13]. This experiment was designed and executed in 1985 to verify the calculation accuracy related to the neutronic design of the Japanese High-Temperature Engineering Test Reactor (HTTR). Whereas the HTTR experiments included several complex design and operational features, the VHTRC facility was specifically designed as a criticality validation benchmark and design verification for the HTTR and, as such, was well-instrumented. An effort was also made to record and quantify experimental uncertainties. The layout of the VHTRC assembly is shown in Figure 9.
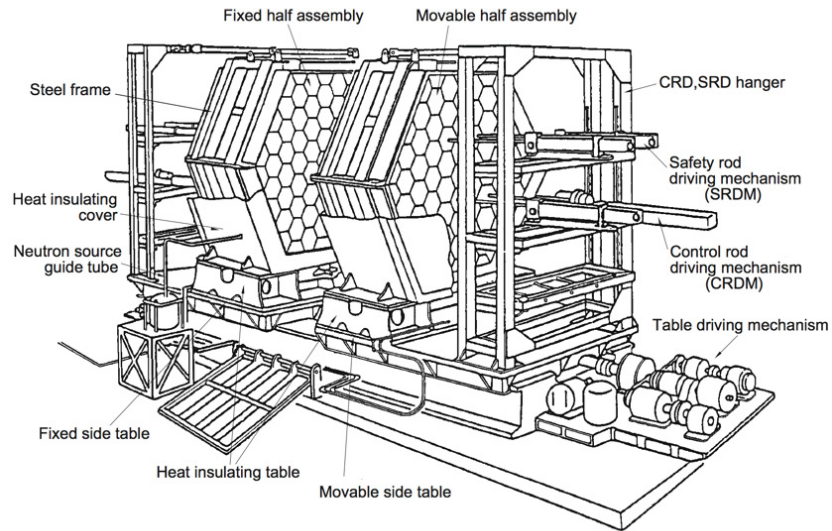
Figure 9. VHTRC assembly layout.

The VHTRC assembly consists of pin-in-block type fuel using carbon-coated particles of low-enriched uranium dioxide (2 and 4 wt%) and a graphite reflector. It has a hexagonal prism shape (2.4 m across the flats and 2.4 m long) and is covered with 0.5-mm-thick Cd sheets as a thermal neutron absorber in the radial direction. The assembly is composed of two axially jointed hexagonal-prism half assemblies, one of which is fixed and one that is movable. The core loading pattern of one of the three core configurations is shown in Figure 10.
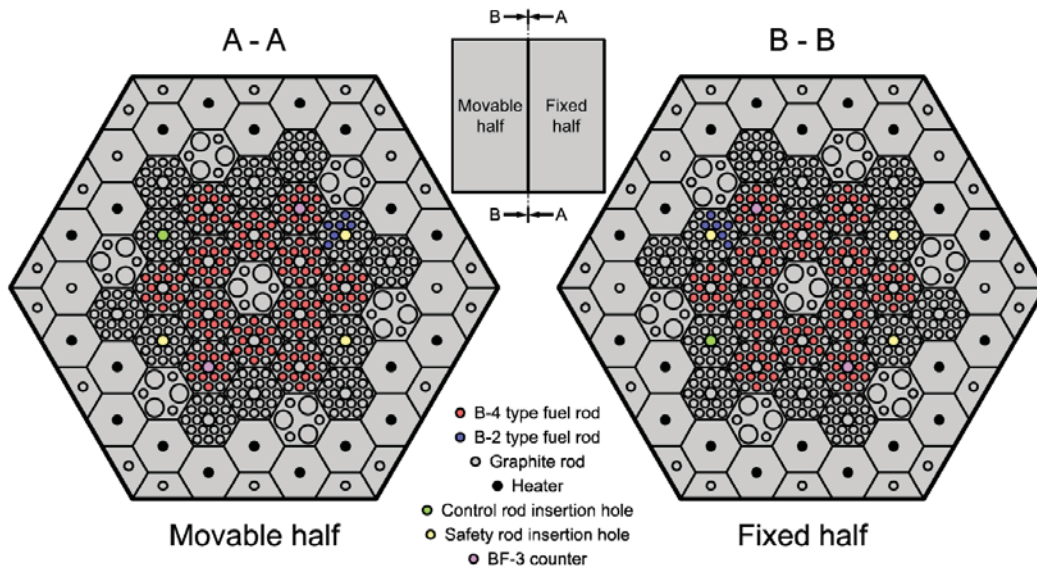
Figure 10. VHTRC HP core loading pattern [13].

In addition to performing critical measurements at room temperature (25.5°C), four measurements at 71.2°C, 100.69°C, 150.5°C, and 199.6°C were performed to determine the temperature effect on reactivity. Furthermore, criticality was reached for the HC-1 and HC-2 core configurations at 8°C and 200.3°C, respectively. All of these configurations have been evaluated and accepted and as benchmark experiments for calculations of temperature-dependent effective multiplication factors and temperature reactivity coefficients, and the configurations have been included in the latest release of the *International Handbook of Evaluated Reactor Physics Benchmark Experiments* [14]. The handbook includes all of the relevant data required to construct detailed simulation models of the experiments, and it can be obtained from the NEA/OECD databank.

Participants are requested to perform nominal (best-estimate) calculations for the multiplication factor, as well as the quantification of cross-section and manufacturing uncertainties. Material uncertainties are provided in Table D-6 and Table D-7, and uncertainties of dimensions can be found in Table 1.1-5 of the VHTRC specifications. The uncertainty variances obtained will be compared with the benchmark uncertainties obtained at this facility and with results obtained in Exercise I-2.

It should be noted that an earlier draft version of these *International Handbook of Evaluated Reactor Physics Benchmark Experiments* specifications used different material compositions for the graphite rods, the reflector and fuel blocks, and end caps. In the final version, these materials have been condensed into a single material. Hence, apart from the graphite in the TRISO particles, only two graphite materials have to be distinguished. Participants should therefore use the 2013 version of this specification.

For the purposes of this CRP, the following simplifications can be implemented in the model of the VHTRC:

- The specifications describe a small space of less than 1 mm between the fuel/graphite rods and the block graphite. To simplify the model, this space must be filled with block graphite. This simplification offers the opportunity to model the blocks that contain only graphite rods as a solid hexagonal graphite block, since the rod and the block material are identical.

- The carbon in all materials should be considered as graphite, i.e., always apply the thermal scattering library for graphite.

10. EXERCISES I-3 AND I-4: LOCAL STAND-ALONE FUEL THERMAL-HYDRAULICS

These exercises are focused on the localized stand-alone fuel thermal response. The aim of the stand-alone thermal unit cell calculations is to isolate the effect of material and boundary input uncertainties on very simplified problems before the same input variations are applied to complex core problems (Phases II–IV). Exercise I-3 requires a steady-state solution for a single fuel compact and coolant channel unit cell with a fixed bulk-coolant temperature, while Exercise I-4 requires the time-dependent solution of the same cell definition combined with a power transient. The figures of merit for both exercises are the variation in the unit cell temperature profiles due to input uncertainty variations in the material properties and boundary conditions. No output parameters will be propagated into subsequent exercises or phases, but the same material input uncertainties (also called manufacturer uncertainties) will be specified in the subsequent phases.

10.1 Exercise I-3

A typical hexagonal MHTGR-350 unit cell is shown in Figure 11, consisting of a helium coolant channel, six fuel compacts, and a matrix graphite region. The helium gaps around the fuel compacts are also included. The equivalent triangular unit cells are shown in Figure 12. The only difference between the two sub-exercises is the representation of the fuel region.

- *Exercise I-3a*: The fuel region is modeled as a volume-averaged homogenous mixture consisting of matrix graphite and TRISO fuel kernels.

- *Exercise I-3b*: The fuel region is modeled as a heterogeneous mixture of TRISO fuel kernels embedded in matrix graphite, i.e., the uranium carbide ($UC_{0.5}O_{1.5}$), inner and outer pyrolitic carbon (IPyC/OPyC), and silicon carbide (SiC) layers of the TRISO fuel particles are explicitly modeled.
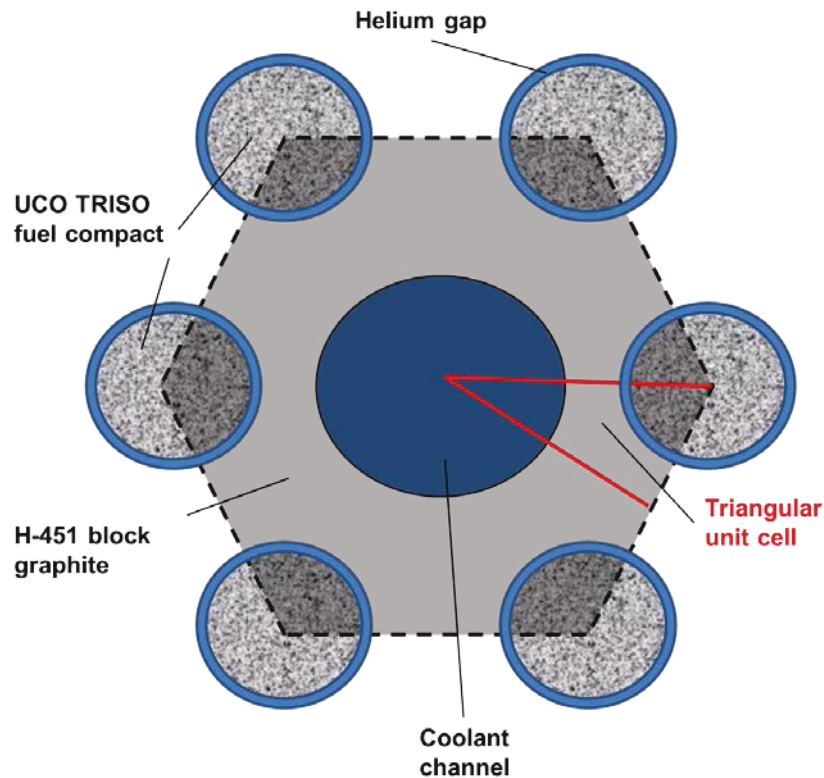
Figure 11. MHTGR-350 hexagonal and triangular unit cell representations.
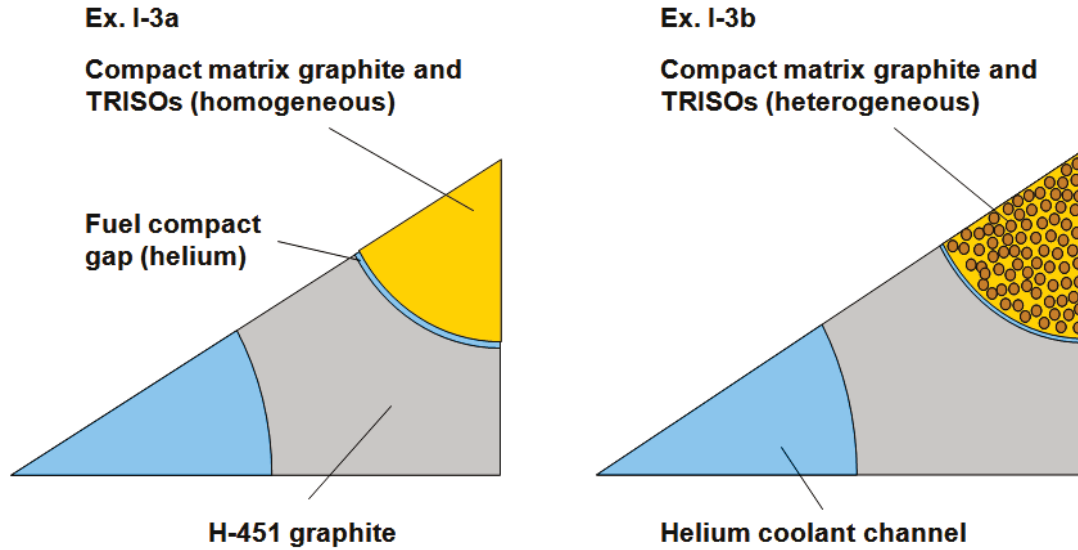
Figure 12. MHTGR-350 triangular unit cells for Exercises I-3a/4a and I-3b/4b.

The geometry and material properties are based on the MHTGR-350 MW benchmark specification [5]. The fuel-lattice unit cell is assumed to be a two-dimensional symmetric 1/12th model of the MHTGR-350 design, with dimensions as shown in Figure 13.
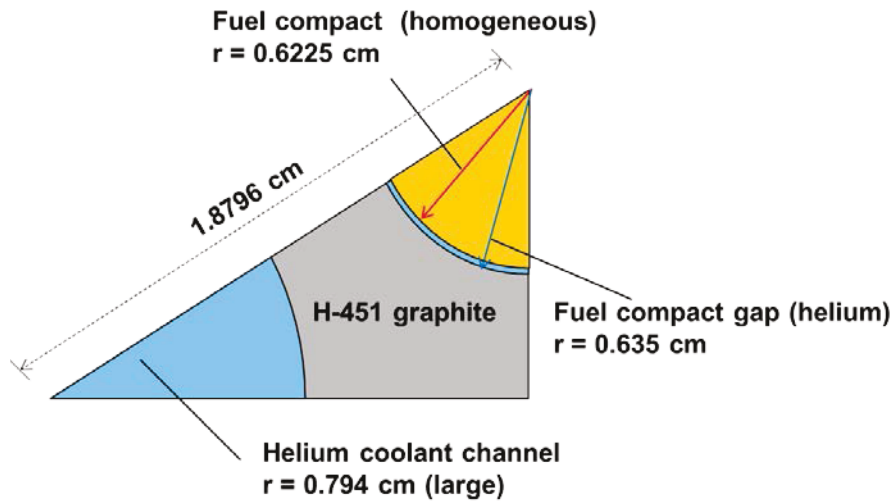
Figure 13. MHTGR-350 triangular unit cell specification.

The following assumptions and input boundary conditions are made:

- There are 102 large and six small coolant holes per standard fuel element. For this exercise, only the large coolant hole geometry will be investigated, i.e., r = 0.794 cm.

- The coolant channel is not implicitly included in the unit cell. This is instead modeled as a simple heat sink boundary with a bulk coolant temperature of 750 K and a constant heat transfer coefficient of 1,700 W/m^2·K.

- The heat transfer coefficient value (1,700 W/m^2·K) is calculated based on nominal MHTGR-350 operating conditions at a pressure of 6.39 MPa using standard pipe flow correlations. The Petukhov correlation has been used to calculate the Darcy friction factor and the Gnielinski correlation [15] has been used to calculate the Nusselt number at a Reynolds number of 43,000.

- The remaining boundaries of the model are assumed adiabatic, i.e., heat conduction to adjacent unit cells is ignored.

- A fixed power density in the fuel compact of 26 MW/m^3 is used. This is based on the nominal modular high-temperature reactor operating power of 350 MW assuming a uniform power distribution. A schematic representation of these nominal case values are shown in Figure 14.

- Heat transfer across the 0.125-mm gap between the fuel compact and H-451 graphite region is modeled assuming heat conduction through stagnant helium and radiative heat transfer using an emissivity value of 0.85 for H451 graphite.

- The complex dependence of the thermal conductivity on temperature and fluence requires specific attention. The same correlations prescribed for the OECD MHTGR-350 benchmark [5] are used in this CRP on HTGR UAM specification. The thermal conductivity, specific heat correlations, and density data are presented in Appendix A for all relevant materials.

- In the case of the fuel compact and the fine-scale behavior of the TRISO particles, the AMEC approach [16] is recommended to determine the "effective" thermal conductivity. This approach is described in Appendix A. An example of the application of this methodology with the OpenFOAM multi-physics toolkit can be found in Clifford et al. [17]. Note, however, that the AMEC methodology is not required to be implemented if participants want to use other methods of determining the effective conductivity of the mixed fuel and graphite media.
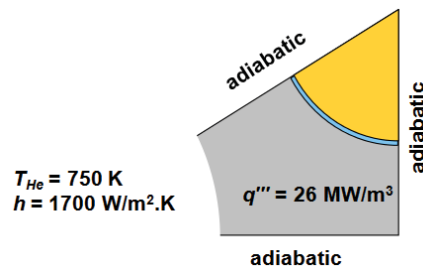
Figure 14. MHTGR-350 unit cell boundary conditions.

The reference (or nominal) calculations for these exercises will be provided by a detailed finite element or finite volume calculation (e.g., utilizing the OpenFOAM multi-physics framework [17]).

The nominal (i.e., best-estimate, expected or mean) values to be used as input for Exercises I-3 and I-4 are included in Table 12. The uncertainty information is specified in Table C-5 (Appendix C).

Table 12. Exercises I-3 and I-4 input parameters – nominal values.

Input Parameter	Nominal/Mean Value
Boundary conditions	
Fuel compact power density	26 MW/m^3
Helium coolant temperature	750 K
Heat transfer coefficient	1,700 W/m^2·K
TRISO packing fraction	0.35
Fuel compact/graphite gap width	0.125 mm
Material properties[a]	
Thermal conductivities	Correlations specified in Appendix A
Specific heat (includes density as ρc_p)	Correlations specified in Appendix A
Emissivity	0.85
Graphite matrix density (kg/m^3)	1,450
H-451 block graphite density (kg/m^3)	1,850
Coated TRISO particles properties	
UC$_{0.5}$O$_{1.5}$ kernel diameter (μm)	425
Buffer thickness (μm)	100
IPyC thickness (μm)	40
SiC thickness (μm)	35
OPyC thickness (μm)	40
UC$_{0.5}$O$_{1.5}$ kernel density (kg/m^3)	10,400
Buffer density (kg/m^3)	1,050
IPyC density (kg/m^3)	1,900
SiC density (kg/m^3)	3,190
OPyC density (kg/m^3)	1,900

a. The uncertainty information originally only applied for NBG-18 graphite, but due to a lack of data for the TRISO coatings, the same variations are assumed for these materials at this stage.

A summary of the input uncertainty parameters, the output parameters that will be compared, and the propagated parameters that will be used in subsequent exercises of the benchmark is presented for Exercise I-3 in Table 13.

Table 13. Summary of input, output, and propagated uncertainty parameters for Exercise I-3.

Input Uncertainty Parameters (I)	Output Parameters to be Compared (O)/Figure of Merit	Propagated Parameters (U)
Material properties (conductivity, specific heat, density, packing fraction)	Solid temperature profiles	None
Boundary conditions (helium coolant temperature, heat transfer coefficient, fuel power level)		

The variation of input material properties accounts for variances that appear during the manufacturing of the fuel and graphite material, while the variation in the boundary conditions accounts for the different conditions that such a unit cell might experience depending on its location in the core (localized variations in coolant flow, power density, etc.).

The required output (steady-state solid temperature) is defined as follows:

- Exercise I-3a:

  - Average and maximum homogeneous fuel region temperature (in neutronic terms – the "Doppler" temperature). In these cases where the TRISO fuel particles are not explicitly modeled, the maximum fuel temperature will be the spatial maximum temperature of the homogenous fuel region.

  - Average temperature of the H-451 graphite region outside the fuel region (in neutronic terms – the "moderator" temperature).

- Exercise I-3b:

  - Volume-average and maximum heterogeneous fuel region temperature. In these cases where the TRISO fuel particles are explicitly included, the maximum fuel temperature will be the UO_2 fuel kernel temperature of the hottest TRISO particle.

  - Average temperature of the H-451 graphite region outside the fuel region.

10.2 Exercise I-4

For Exercise I-4 a fictitious power excursion transient is defined to act as a time dependent source. All other parameters remain identical to the values specified for Exercise I-3. Two sub-cases are also defined here, corresponding to the homogeneous (Exercise I-4a) and heterogeneous (Exercise I-4b) fuel region modeling. The power transient is defined as follows:

- Over the first 2 seconds of the transient the power increases linearly up to 10x the nominal power (i.e., 260 MW/m^3).

- Between 2 s and 30 s, the power decreases exponentially according to the following equation:

$$P(t) = 10 P_0 e^{-0.2(t-2)}$$

(1)

The transient calculation is terminated at 30 s. The resulting time-dependent input power profile is shown in the figure below.
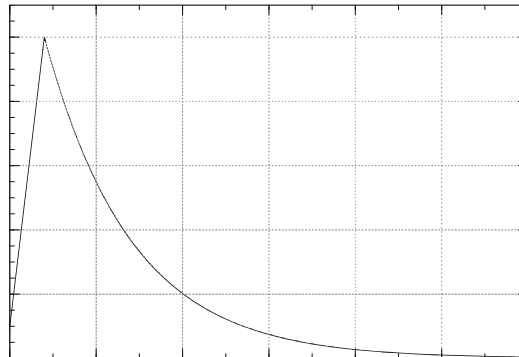
Figure 15. Transient power profile definition for Exercise I-3.

A summary of the input uncertainty parameters, the output parameters that will be compared, and the propagated parameters that will be used in subsequent exercises of the benchmark is presented for Exercise I-4 in Table 14. The input parameter variation specified in Table 12 must also be applied for Exercise I-4.

Table 14. Summary of input, output, and propagated uncertainty parameters for Exercise I-4.

Input Uncertainty Parameters (I)	Output Parameters to be Compared (O)	Propagated Parameters (U)
Material properties (conductivity, specific heat, density, packing fraction)	Time-dependent solid temperature profiles	None
Boundary conditions (helium coolant temperature, heat transfer coefficient, steady-state fuel power level)	Time point of peak fuel temperature	

The required output (steady-state solid temperature) is defined as follows:

- Exercise I-4a:

  - Average and maximum time-dependent homogeneous fuel region temperature. The maximum fuel temperature for Exercise I-4a will be the spatial maximum temperature of the homogenous fuel region.

  - Average time-dependent temperature of the H-451 graphite region outside the fuel region.

- Exercise I-4b:

  - Volume-average and maximum time-dependent heterogeneous fuel region temperature. The maximum fuel temperature for Exercise I-4b will be the UO_2 fuel kernel temperature of the hottest TRISO particle (typically in the center of the fuel region).

  - Average time-dependent temperature of the H-451 graphite region outside the fuel region.

11. SUMMARY

The specifications for all the prismatic high-temperature reactor exercises included in Phase I of the CRP on HTGR UAM were presented. The information included exercise descriptions, neutronic and thermal-hydraulic data sets, support data, and required results. This document will be updated with participants' comments after the 3rd RCM, planned for May 2015 in Idaho Falls, Idaho, if required.

12. REFERENCES

1. International Atomic Energy Agency, *Evaluation of high temperature gas cooled reactor performance: Benchmark analysis related to initial testing of the HTTR and HTR-10*, IAEA-TECDOC-1382, November 2003, pp. 346.

2. F. Reitsma, et al., "The OECD/NEA/NSC PBMR400 MW coupled neutronics thermal hydraulics transient benchmark – Steady-state results and status," *Proceedings of PHYSOR-2008 Conference, International Conference on the Physics of Reactors, "Nuclear Power: A Sustainable Resource," Casino-Kursaal Conference Center, Interlaken, Switzerland*, September 14-19, 2008.

3. G. Strydom, et al., "THE OECD/NEA/NSC PBMR 400 MW Coupled Neutronics Thermal Hydraulics Transient Benchmark: Transient Results," *Proceedings of PHYSOR-2010 Conference, International Conference on the Physics of Reactors, Pittsburgh, PA, USA*, May 2010.

4. K. Ivanov, et al., "Benchmark for Uncertainty Analysis in Modelling (UAM) for Design, Operation and Safety Analysis of LWRs," *Volume I: Specification and Support Data for the Neutronics Cases (Phase I), Version 2.0*, OECD Nuclear Energy Agency NEA/NSC/DOC(2013)7, May 2013.

5. J. Ortensi, et al., *Prismatic Coupled Neutronics/Thermal Fluids Transient Benchmark of the MHTGR-350 MW Core Design: Benchmark Definition*, OECD Nuclear Energy Agency NEA/NSC/DOC(2013), DRAFT (03/01/2013).

6. F. Reitsma and B. Tyobeka, "Current Status and Results of the PBMR 'Pebble Box' Benchmark within the Framework of the IAEA CRP5," *Proceedings of PHYSOR 2010 Pittsburgh, Pennsylvania, USA*, 2010.

7. B. Tyobeka and F. Reitsma, "Results of the IAEA CRP5 - Benchmark Analysis Related to the PBMR-400, PBMM, GT-MHR, HTR-10 and the ASTRA Critical Facility," *Proceedings of PHYSOR 2010 Pittsburgh, Pennsylvania, USA*, 2010.

8. F. Bostelmann, G. Strydom, and Su Jong Yoon, *Results for Phase I of the IAEA Coordinated Research Program on HTGR Uncertainties*, INL/EXT-14-32944, Rev. 1, January 2015.

9. I. Kodeli, "Multidimensional Deterministic Nuclear Data Sensitivity and Uncertainty Code System: Method and Application," *Nuclear Science and Engineering*, Vol. 138, pp. 45–66, 2001.

10. B. Rearden et al, "Applications of the TSUNAMI Sensitivity and Uncertainty Analysis Methodology," *Proceedings of the 7th International Conference on Nuclear Criticality Safety ICNC2003; Challenges in the Pursuit of Global Nuclear Criticality Safety,* Techno Community Square Ricotti, Tokai, Ibaraki, Japan, October 20–24, 2003.

11 V. Descotes, et al., "Studies of 2D Reflector Effects in Cross-Section Preparation for Deep Burn VHTRs," *Nuclear Engineering and Design*, Vol. 242, pp. 148–156, 2012.

12. J. M. Noh, et al. "Development of a Computer Code System for the Analysis of Prism and Pebble Type VHTR Cores," *Annals of Nuclear Energy*, Vol. 35**,** pp. 1919–1928, 2008.

13. NEA, "Temperature effect on reactivity in VHTRC 1 core," VHTRC GCR EXP 001, CRIT COEF, NEA/NSC/DOC(2006)2, 2006.

14. NEA, *International Handbook of Evaluated Reactor Physics Benchmark Experiments*, NEA No. 7140, March 2013.

15. F. Incropera and D. DeWitt, *Fundamentals of Heat and Mass Transfer*, 6th ed., New York: Wiley, 2007.

16. R. Stainsby, et al., *Investigation of Local Heat Transfer Phenomena in a Prismatic Modular Reactor Core*, NR001/RP/001 R1, AMEC NSS Limited, 2009.

17. I. Clifford, K. Ivanov, and M. Avramova, "A Multi-Scale Homogenization and Reconstruction Approach for Solid Material Temperature Calculations in Prismatic High Temperature Reactor Cores," *Nuclear Engineering and Design*, Vol. 256, pp. 1–13, 2013.

Appendix A

Fuel and Graphite Thermo-Physical Properties

The complex dependence of the graphite thermal conductivity on temperature and fluence requires specific attention. The same correlations prescribed for the OECD MHTGR-350 benchmark [1] are used in this CRP on HTGR UAM specification. A summary of these correlations are presented here for all fuel and graphite materials. The correlations are provided for use in Exercises I-3 and I-4.

A-1. GRADE H-451 GRAPHITE

For this benchmark, all material thermodynamic properties are assumed isotropic. Table A-1 and Figure A-1 show that considerable thermal conductivity dependence exists on the fluence level, varying by almost 300% at 1,000 K between zero and 8×10^{25} n/m^2. If implemented as a statistical uncertainty in this UAM specification, this parameter will therefore dominate all other uncertainties (specifically in the transient cases). The variation in fluence is a function of the operational history of the reactor and, as such, will exhibit spatial and temporal variations. For the Phase II specifications, a full spatially dependent fluence distribution will be provided, but for the Phase I specification, only a "representative" unit cell approach is desired. The fluence point closest to the preferred range of the AGR-1 fuel irradiation program [2] is 3×10^{25} n/m^2, and this value has therefore been chosen to represent the "expected" or best-estimate value of the H-451 graphite thermal conductivity. Nevertheless, it remains an issue how to specify the effect of fluence on thermal conductivity in a statistically consistent manner.

Table A-1. Thermo physical properties of grade H-451 graphite.

Parameter	Value[a]
Thermal conductivity [W/m/K]	$k = 4.19346 \times 10^{-6} T^2 - 2.13523 \times 10^{-2} T + 5.41993 \times 10^1$
Density (kg/m^3)	1,850
Specific heat (J/kg.K)	$C_p = \begin{pmatrix} 0.54212 - 2.42667 \times 10^{-6} T - 90.2725 T^{-1} - 43449.3 T^{-2} \\ +1.59309 \times 10^7 T^{-3} - 1.43688 \times 10^9 T^{-4} \end{pmatrix} \cdot 4184$
Emissivity	0.85
a. Empirical data range [500 K – 1,800 K], T in K. Fluence point chosen at 3×10^{25} n/m^2.	
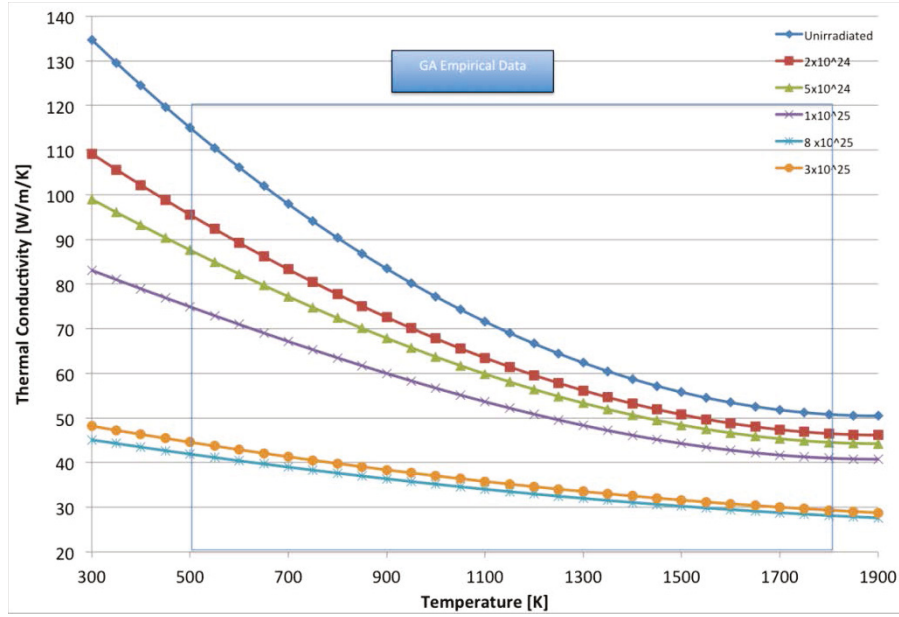
Figure A-1. Thermal conductivity of Grade H-451 graphite.

A-2. PYROLITIC CARBON LAYER

The TRISO particles include an outer and inner pyrolitic carbon layer that surrounds the SiC layer and provide structural support. A porous carbon layer is positioned between the kernel and the inner pyrolitic carbon to retain fission gases (also called the "buffer layer"). The thermo-physical properties of the PyC and porous carbon layers are included in Table A-2.

Table A-2. Pyrolitic and porous carbon thermo-physical properties.

Property	Value
Thermal conductivity (W/m/K)	$k_{PyC} = 244.3 T^{-0.574} \left[1 - 0.3662 \left(1 - e^{-1.005\Gamma} \right) - 0.03554\Gamma \right]$ $\left[\dfrac{\rho_{PyC}}{2.2 \left(1930 - \rho_{PyC} \right) + \rho_{PyC}} \right]$ $k_{PC} = 122.15 T^{-0.574} \left[1 - 0.3662 \left(1 - e^{-1.005\Gamma} \right) - 0.03554\Gamma \right]$ $\left[\dfrac{\rho_{PC}}{2.2 \left(1930 - \rho_{PC} \right) + \rho_{PC}} \right]$ Γ = neutron fluence = 3×10^{25} n/m² DNE
Density PyC (kg/m³)	1,900
Density porous C (kg/m³)	1,050
Specific heat (J/kg/K)	$C_p = \left(\begin{array}{c} 0.54212 - 2.42667 \times 10^{-6} T - 90.2725 T^{-1} - 43449.3 T^{-2} \\ + 1.59309 \times 10^{7} T^{-3} - 1.43688 \times 10^{9} T^{-4} \end{array} \right) \cdot 4184$

A-3. FUEL COMPACT MATRIX GRAPHITE

The fuel compact consists of a large number of TRISO-coated particles embedded in a graphite matrix. The thermo-physical properties for the graphite matrix material are included Table A-3.

Table A-3. Compact matrix graphite thermo-physical properties.

Property	Value
Thermal conductivity (W/m/K)	$k = 47.4 \cdot \left(1 - 9.7556 \cdot 10^{-4} \cdot (T - 373.15) \cdot e^{-6.036 \cdot 10^{-4}(T-273.15)}\right)$ $\left[1 - 0.3662\left(1 - e^{-1.005\Gamma}\right) - 0.03554\Gamma\right]\left[\dfrac{\rho}{2.2(1700 - \rho) + \rho}\right]$ Γ = neutron fluence = 3×10^{25} n/m^2 Dido Nickle Equivalent
Density matrix (kg/m^3)	1,450
Specific heat (J/kg/K)	$C_p = \left(\begin{array}{l} 0.54212 - 2.42667 \times 10^{-6} T - 90.2725 T^{-1} - 43449.3 T^{-2} \\ +1.59309 \times 10^{7} T^{-3} - 1.43688 \times 10^{9} T^{-4} \end{array}\right) \cdot 4184$

A-4. SIC LAYER

The thermo-physical properties for the SiC layer are shown in Table A-4.

Table A-4. SiC thermo physical properties.

Property	Value
Thermal conductivity (W/m/K)	$k = \left(\dfrac{17885}{T} + 2\right) e^{-0.1277\Gamma}$ Γ = neutron fluence = 3×10^{25} n/m^2 DNE
Density (kg/m^3)	3,190
Specific Heat (J/kg/K)	$C_p = 925.65 + 0.3772 T - 7.9259 \times 10^{-5} T^{2} - \dfrac{3.1946 x 10^{7}}{T^{2}}$

A-5. UC$_{0.5}$O$_{1.5}$ KERNEL

Since no data are available for UC$_{0.5}$O$_{1.5.}$, uranium dioxide (UO$_2$) properties will be used instead.

A-5.1 Thermal Conductivity of UO$_2$

The model for irradiated UO$_2$ thermal conductivity is specified below:

$$k(T, B, p) = k_0(T) * FD * FP * FR \qquad \text{[W/m.K]} \qquad \text{(A-1)}$$

where

T = temperature [K]

B = burnup [at. %]

P = porosity of UO$_2$ [unit less]

ρ = density of UO$_2$ [kg/m^3]

ρ_{TD} = theoretical density of UO_2 [kg/m³]

k_o = conductivity of 100% dense UO_2 [W/m/K]

FD = dissolved solid fission product factor [unit less]

FP = precipitated solid fission product factor [unit less]

FR = radiation damage factor [unit less]

$$p = \frac{\rho_{TD} - \rho}{\rho_{TD}} = 0$$

$$t = \frac{T(K)}{1000}$$

$$k_0(T) = \frac{115.8}{7.5408 + 17.692t + 3.6142t^2} + 7410.5t^{-5/2}e^{-16.35/t}$$

$$FD = \left(\frac{1.09}{B^{3.265}} + 0.0643\sqrt{\frac{T}{B}}\right)\arctan\left[\left(\frac{1.09}{B^{3.265}} + 0.0643\sqrt{\frac{T}{B}}\right)^{-1}\right]$$

$$FP = 1 + \frac{0.019B}{3 - 0.019B}\left[1 + e^{-(T-1200)/100}\right]^{-1}$$

$$FR = 1 - \frac{0.2}{1 + e^{(T-900)/80}}$$

A-5.2 Heat Capacity of UO2

The specific heat capacity model covers the temperature range 298.15 K ≤ T < 3120 K, and it is functionalized as:

$$C_p(T) = 302.27\left(\frac{548.68}{T}\right)^2 \frac{e^{548.68/T}}{\left(e^{548.68/T} - 1\right)^2} + 2*C_2(B)T + 8.741\times10^7 * 18531.7\frac{e^{-18,531.7/T}}{T^2}$$

(A-2)

where

$C_p(T)$ = specific heat capacity [J/kg·K]

T = Temperature [K]

$C_2(B) = 8.463x10^{-03}(1 + 0.011*B)$ [at. %]

B = burnup [at. %].

A-5.3 Density of UO2

Participants should use the fixed value ρ= 10,400 kg/m³. Dimensional changes in the kernel density with temperature are not taken into account.

A-6. EFFECTIVE PROPERTIES FOR TRISO PARTICLES

The effective thermal conductivity of the TRISO particles is computed with

$$k_{eff,TRISO} = k_m \left(\frac{1-2B_{(N_{coat}+2)}}{1+B_{(N_{coat}+2)}} \right) \tag{A-3}$$

where k_m is the conductivity of the graphite matrix and $B_{(N_{coat}+2)}$ is the coefficient obtained from inverting the matrix system that represents the various TRISO coatings as developed by AMEC/NSS [3]. The actual matrix shown in Reference 3 is in error. The correct matrix is given in Figure A-2 for four coatings ($N_{coat} = 4$).

$$\begin{bmatrix}
1 & -1 & & & & & & \frac{a_5^3}{a_1^3} & -\frac{a_5^3}{a_1^3} & & & \\
 & 1 & -1 & & & & & \frac{a_{(N_{coat}+1)}^3}{a_2^3} & -\frac{a_5^3}{a_2^3} & & & \\
 & & 1 & -1 & & & & \frac{a_5^3}{a_3^3} & -\frac{a_5^3}{a_3^3} & & & \\
 & & & 1 & -1 & & & & \frac{a_5^3}{a_4^3} & -\frac{a_5^3}{a_4^3} & & \\
 & & & & 1 & -1 & & & & 1 & -1 \\
 & & & & & 1 & & & & & 0 \\
 & & & & & & 1 & & & & \\
0 & & & & & & & -2\frac{a_5^3}{a_1^3}k_1 & 2\frac{a_5^3}{a_1^3}k_2 & & \\
k_1 & -k_2 & & & & & & & & & \\
 & k_2 & -k_3 & & & & & -2\frac{a_5^3}{a_2^3}k_2 & 2\frac{a_5^3}{a_2^3}k_3 & & \\
 & & k_3 & -k_4 & & & & & -2\frac{a_5^3}{a_3^3}k_3 & 2\frac{a_5^3}{a_3^3}k_4 & \\
 & & & k_4 & -k_5 & & & & & -2\frac{a_5^3}{a_4^3}k_4 & 2\frac{a_5^3}{a_4^3}k_5 \\
 & & & & k_5 & -k_6 & & & & & -2k_5 & 2k_6
\end{bmatrix}$$

Figure A-2. Corrected matrix for the AMEC compact model.

The effective specific heat capacity is computed with a scheme based on balance of energy and the effective density with a scheme based on balance of mass:

$$Cp_{eff} = \frac{\int \rho Cp \, dV}{\int \rho \, dV} \qquad \rho_{eff} = \frac{\int \rho \, dV}{\int dV} \tag{A-4}$$

A-7. EFFECTIVE PROPERTIES FOR FUEL COMPACTS

The thermal conductivity of fuel compacts is computed with:

$$k_{eff,compact} = k_m \left(\frac{1 - 2\alpha B_{(N_{coat}+2)}}{1 + \alpha B_{(N_{coat}+2)}} \right)$$

(A-5)

where k_m is the conductivity of the graphite matrix, α is the volume fraction occupied by the TRISO particles, and $B_{(N_{coat}+2)}$ is the coefficient obtained from inverting the matrix system that represents the various TRISO coatings [3].

The effective specific heat capacity is computed with a scheme based on balance of energy and the effective density with a scheme based on balance of mass, as shown above.

A-8. EFFECTIVE PROPERTIES FOR THERMAL UNIT CELLS

The thermal conductivity model of the thermal unit cell is based on Maxwell's theory of the conductivity of composite materials. The original theory is derived for two materials, but it is extended to three materials for the HTGR applications by AMEC/NSS [3]. The effective **radial** conductivity of a thermal unit cell is given by the following expression:

$$k_{eff} = k_s \left\{ 1 - \frac{2\left[\alpha_1 \left(k_s - k_{por}\right)\left(k_s + k_{FC}\right) + \alpha_2 \left(k_s - k_{FC}\right)\left(k_s + k_{por}\right) \right]}{\left[\left(k_s + k_{por}\right)\left(k_s + k_{FC}\right) + \alpha_1 \left(k_s - k_{por}\right)\left(k_s + k_{por}\right) + \alpha_2 \left(k_s - k_{FC}\right)\left(k_s + k_{por}\right) \right]} \right\}$$

(A-6)

where

k_{eff}	=	effective radial thermal conductivity of the cell
k_s	=	thermal conductivity of the graphite
k_{por}	=	thermal conductivity of the matrix material
k_{FC}	=	thermal conductivity of the fuel compact
α_1	=	volume fraction of gap material
α_2	=	volume fraction of fuel compacts.

The effective **axial** conductivity of a thermal unit cell is given with the following expression:

$$k_{eff,axial} = k_s \alpha_3 + k_{FC} \alpha_2 + k_{por} \alpha_1$$

(A-7)

where α_3 = volume fraction of graphite

The effective specific heat capacity is computed with a scheme based on balance of energy and the effective density with a scheme based on balance of mass:

$$Cp_{eff} = \frac{\int \rho Cp \, dV}{\int \rho \, dV} \qquad \rho_{eff} = \frac{\int \rho \, dV}{\int dV}$$

(A-8)

REFERENCES

1. J. Ortensi, et al., *Prismatic Coupled Neutronics/Thermal Fluids Transient Benchmark of the MHTGR-350 MW Core Design: Benchmark Definition*, OECD Nuclear Energy Agency NEA/NSC/DOC(2013), DRAFT (03/01/2013).

2. J. T. Maki, *AGR-1 Irradiation Experiment Test Plan*, INL/EXT-05-00593, Rev. 3, 2009.

3   R. Stainsby, et al., *Investigation of Local Heat Transfer Phenomena in a Prismatic Modular Reactor Core*, NR001/RP/001 R1, AMEC NSS Limited, 2009.

Appendix B

Phase I Output Reporting

Participants are requested to provide the following parameters for comparison of Exercise I-1 and Exercise I-2:

- k_∞ and the standard deviation of k_∞ due to the cross-section covariance data. (The unit provided in Tsunami (%$\Delta k/k$) is requested for submission.)

- The top five nuclide-reaction contributors of the uncertainty in k_∞. This will allow participants to identify reactions that contribute most to the total uncertainties. The fractional values for the five contributors (called "varfrac" in the submission template) are available in the standard TSUNAMI output (the unit is fractions of %$\Delta k/k$, so it can be listed as-is). For any other submissions—for example, the sample-based approach (e.g., SAMPLER or XSUSA)—participants must provide these contributors together with the applied formulation, because these definitions/interpretations might vary between codes.

- One-group microscopic cross sections (barns), as listed in Table B-1. The one-group cross sections are obtained by collapsing the fine group cross sections into a single group (e.g., available in NEWT using the "prtbroad" and "collapse" parameters).

Table B-1. Requested one-group microscopic cross-sections for Phase I.

Output Identifier (in template)	Description	Notes
fuel_mic_n_gam_235U	^{235}U n,γ (mt=102)	Fuel region only
fuel_mic_n_gam_238U	^{238}U n,γ (mt=102)	Fuel region only
fuel_mic_fiss_235U	^{235}U fission (mt=18)	Fuel region only
fuel_nu_bar_235U	^{235}U average number of neutrons per fission (mt=452)	Fuel region only
mod_mic_inelastic_12C	^{12}C total in-elastic scatter (mt=2)	Moderator region only. Total inelastic scattering of all ^{12}C atoms in the TRISO fuel, fuel compact graphite matrix, and fuel block graphite. Corresponds to total moderator contribution. For Exercise I-2c, the contribution of the reflector blocks (i.e., non-fuel blocks) should NOT be included (see below).
refl_mic_inelastic_12C	reflector-only: ^{12}C total in-elastic scatter (mt=2)	Only for Exercise I-2c reflector region. Total inelastic scattering of all ^{12}C atoms in the reflector block graphite. Corresponds to total reflector contribution. The contribution of all fuel graphite (i.e., TRISO+matrix+fuel H-451) should be excluded here and listed as described above.
fuel_mic_n_gam_239Pu	fuel-only: ^{239}Pu n,γ (mt=102)	Only for Exercise I-2b and Exercise I-2c fuel region.
fuel_nu_bar_239Pu	fuel-only: ^{239}Pu average number of neutrons per fission (mt=452)	Only for Exercise I-2b and Exercise I-2c fuel region.

- The standard deviations for the one-group cross sections. If TSUNAMI is used, these data can be obtained for each nuclide reaction by using the "system responses" option, as shown in example T1.6.9 of the user manual.

- The compact power densities for the five positions shown in Figure 4, as well as the associated standard deviations (in W/cm^3).

Examples of completed results and instruction pages for Exercise I-1a are provided in Figure B-1 and Figure B-4, respectively. The Excel files for the Exercise I-1a example and the empty templates for Exercise I-1a to Exercise I-2c are embedded here as Figure B-2 and Figure B-3, respectively. Participants can also request these files via e-mail from the IAEA CRP coordinator.

OUTPUT SUMMARY						
output	value	absstd	relstd (%)		case	I-1a.CZP
k	1.04587E+00	5.10000E-03	4.87633E-01		participant	INL-TSU-CE-IFP
fuel_mic_n_gam_235U	1.00000E-03	3.10000E-06	3.10000E-01		date	7/6/2015
fuel_mic_n_gam_238U	2.00000E-02	4.10000E-06	2.05000E-02			
fuel_mic_fiss_235U	3.00000E-02	5.10000E-06	1.70000E-02			
fuel_nu_bar_235U	4.00000E-02	6.10000E-06	1.52500E-02			
tot_mic_inelastic_12C	5.00000E-02	7.10000E-06	1.42000E-02			

UNCERTAINTY BREAKDOWN: k			
input	ranking	varfrac	
mt102_238U	1	5.00000E-01	
mt102_235U	2	4.00000E-01	
mt27_238U	3	3.00000E-01	
mt18_235U	4	2.00000E-01	
mt2_12C	5	9.00000E-02	

EXAMPLE

Figure B-1. Example of completed template results page.

Phase_I_ex_1_2_tem
plate_example.xlsx

Figure B-2. Excel file: completed example.

Phase_I_ex_1_2_tem
plate.xlsx

Figure B-3. Excel file: submission templates for Exercise I-1a to Exercise I-2c.

IAEA CRP on HTGR Uncertainties in Modeling			
Submission template: Phase I			
Cells with **BLACK** `(Courier New) text` *are to be filled in.*			
Cells with **BLUE** *text are static. Do not change.*			
Cells with **GREEN** *text are automatically updated based on entered results. Do not change.*			
Key	**Value**		
participant*	`INL-TSU-CE-IFP`		
submission date	`7/6/2015`		
country	`USA`		
institution	`INL`		
author	`G Strydom`		
email	gerhard.strydom@inl.gov		
nuclear data library	`ENDF_VII.1`		
covariance data library	`44 g SCALE`		
computer code	`SCALE`		
calculation methodology	`SCALE/KENO CE, then TSUNAMI`		
uncertainty methodology	`TSUNAMI CE using IFP method, based on adjoint formulation`		
DESCRIPTION OF RESULTS TO BE PROVIDED			
OUTPUT SUMMARY			
Output	*Description*	*Unit*	
k	*eigenvalue/multiplication factor*	-	
fuel_mic_n_gam_235U	*fuel-only, microscopic (1-group) n, γ cross section for 235U*	barns	
fuel_mic_n_gam_238U	*fuel-only, microscopic (1-group) n, γ cross section for 238U*	barns	
fuel_mic_fiss_235U	*fuel-only, microscopic (1-group) fission cross section for 235U*	barns	
fuel_nu_bar_235U	*fuel-only, average number of neutrons per fission for 235U*	barns	
mod_mic_inelastic_12C	*moderator-only, total microscopic (1-group) in-elastic scatter cross section for 12C*	barns	
refl_mic_inelastic_12C	*reflector-only, total microscopic (1-group) in-elastic scatter cross section for 12C*	barns	
fuel_mic_n_gam_239Pu	*fuel-only, microscopic (1-group) n, γ cross section for 239Pu*	barns	
fuel_nu_bar_239Pu	*fuel-only, average number of neutrons per fission for 239Pu*	barns	
For k-inf and all cross-sections above: provide standard deviations (one sigma) in absolute units. Conversion to relative % will be performed automatically			
UNCERTAINTY BREAKDOWN: k			
Provide the nuclide data for the top 5 INPUT PARAMETERS responsible for the uncertainty in k			
in the format, **mtX_AAANm**, where:			
Component	*Description*		
X	*mt number of data, e.g. capture = 101 (see below)*		
AAA	*atomic mass, e.g. 235, 238*		
Nm	*name of nuclide, e.g. U, Pu*		
MT	*Description*		
2	*elastic scattering*		
4	*inelastic scattering*		
16	*n,2n*		
18	*fission*		
27	*absorption*		
101	*capture*		
102	*n,gamma*		
452	*nubar*		
Variance fractions (varfrac) are the fraction of total variance of k due to this input parameter and are optional.			
COMAPCT POWER DENSITIES (Ex. I-2 only)			
Power densities for the 5 positions indicated in Fig. 4 (W/cm³), and associated absolute standard deviations (W/cm3) .			

Figure B-4. Example of completed template instruction page.

Appendix C

Manufacturer and Material Uncertainty Data for Phase I

The manufacturer and material uncertainty data related to the Phase I exercises are provided in this appendix. For the neutronics exercises (I-1 and I-2), the 44 group cross-section co-variance data are accessible through the SCALE code and are not repeated here. In addition to the cross-section uncertainties, various data sources have been used to compile a set of uncertainties related to manufacturer data, material properties, and boundary conditions. Participants should indicate which of these uncertainties they included in their combined analyses if the full set was not used.

The nominal (i.e., best estimate, expected, or mean) and one standard deviation values for the dimensions and number densities used for Exercise I-1a/c are included in Table C-1 and Table C-2, respectively. The respective information for Exercise I-1b/d and also Exercise I-2 is included in Table C-3 and Table C-4.

The nominal (i.e., best-estimate, expected, or mean) and one standard deviation values to be used as input for Exercises I-3 and I-4 are included in Table C-5. The statistical distribution types are Gaussian, unless otherwise indicated.

Uncertainties of the nuclide densities of the VHTRC can be found in Table C-6 and Table C-7.

Table C-1. Dimensions for Exercise I-1a/c - nominal and 1σ uncertainties values.

Parameter	Nominal/Mean Value (mm)	1σ Standard Deviation (mm/%)	Source
Fuel compact outer radius	6.225	0.09	[1]
Helium gap outer radius	6.350	No data	—
Unit cell pitch	1.8796	No data	—
Fuel compact height	49.280	0.32	[1]

Table C-2. Number densities for Exercise I-1a/c - nominal and 1σ uncertainties values.

Nuclide		Nominal/Mean Value (atoms/b·cm)	1σ Standard Deviation Uncertainty	Source
13. Homogenized fuel region	^{235}U	1.5765E-04	± 0.14%	[1]
	^{238}U	8.4864E-04	± 0.14%	[1]
	^{16}O	1.5094E-03	± 0.14%	[1]
	Graphite[a]	6.9958E-02	± 3.22%	Calculated out of all graphite uncertainties in the compact [1]
	^{28}Si	2.8457E-03	± 0.10%	[1]
	^{29}Si	1.4456E-04	± 0.10%	[1]
	^{30}Si	9.5408E-05	± 0.10%	[1]
Coolant channel	^{4}He	2.4600E-05	None	
H-451 block graphite	Graphite[b]	9.2756E-02	± 0.06%	[2]

a. Graphite is defined here as natural carbon including thermal scattering data for graphite. In the SCALE code, this is C-graphite; in Serpent/MCNP, this is natural carbon with the additional thermal scattering data applied. This definition is applied for all neutronics problems in this benchmark. A sensitivity study performed at INL showed minor differences if various mixtures of C-nat and C-graphite are used.

b. In the absence of experimental data, the uncertainty information of the graphite components in the VHTRC are applied for H-451 block graphite.

Table C-3. Dimensions for Exercises I-1b/d and I-2 - nominal and 1σ uncertainties values.

Parameter		Nominal/Mean Value (cm)	1σ Standard Deviation Uncertainty	Source
TRISO fuel particle	$UC_{0.5}O_{1.5}$ kernel radius	2.125E-02	± 2.58%	[1]
	Porous carbon buffer layer outer radius	3.125E-02	± 7.93%	[1]
	Inner PyC outer radius	3.525E-02	± 5.84%	[1]
	SiC outer radius	3.875E-02	± 3.69%	[1]
	Outer PyC outer radius	4.275E-02	± 5.13%	[1]
TRISO packing fraction		0.35	None	—
Fuel compact outer radius		0.6225	± 0.09%	[1]
Helium gap outer radius		0.6350	No data	—
Unit cell pitch		0.9398	No data	—
Fuel compact height		4.928	± 0.32%	[1]

Table C-4. Number densities for Exercises I-1b/d and I-2 - nominal and 1σ uncertainties values.

Number Densities		Nuclide	Nominal/Mean Value (at/b-cm)	1σ Standard Deviation Uncertainty	Source
TRISO fuel particle	Kernel	^{235}U	3.6676E-03	± 0.14%	[1]
		^{238}U	1.9742E-02	± 0.14%	[1]
		^{16}O	3.5114E-02	± 0.14%	[1]
		Graphite	1.1705E-02	± 0.14%	[1]
	Porous carbon	Graphite	5.2646E-02	± 3.64%	[1]
	IPyC	Graphite	9.5263E-02	± 0.74%	[1]
	SiC	^{28}Si	4.4159E-02	± 0.10%	[1]
		^{29}Si	2.2433E-03	± 0.10%	[1]
		^{30}Si	1.4805E-03	± 0.10%	[1]
		Graphite	4.7883E-02	± 0.10%	[1]
	OPyC	Graphite	9.5263E-02	± 0.42%	[1]
Compact matrix		Graphite	7.2701E-02	± 0.63%	[3]
Coolant channels		^{4}He	2.4600E-05	None	—
H-451 block graphite[a]		Graphite	9.2756E-02	± 0.06%	[2]

a. The information of the H-451 block graphite has to be applied to the block graphite in the unit cell and fuel blocks, as well as to the reflector block in the super cell.

NOTE: *Uncertainty estimates are not available for the LBP particles/compact (Exercise I-2a) or the depleted isotopes defined for Exercise I-2b/2c.*

Table C-5. Exercise I-3 and I-4 input parameters – nominal and 1σ uncertainties values.

Input Parameter	Nominal/Mean Value	1σ Standard Deviation Uncertainty	Source
Boundary conditions			
Fuel compact power density	26 MW/m^3	± 2.5%	Total power uncertainty from [4].
Heat transfer coefficient	1,700 W/m^2.K	± 2.5%	Helium conductivity and specific heat uncertainty from [4]. Friction and pipe correlation uncertainty assumed at similar magnitude – to be confirmed.
TRISO packing fraction	0.35	None	Use to assign compact power density to TRISOs.
Fuel compact/graphite gap width	0.125 mm	± 1%	Assumed – to be confirmed.
Material properties[a]			
Thermal conductivities	Correlations specified in Appendix A for each material	± 7%	[4]
Specific heat (includes density as ρc_p)	Correlations specified in Appendix A for each material	± 3%	[4]
Emissivity	0.85	± 3.5%	[4]
Compact matrix density (kg/m^3)	1,450	± 0.63%	[3]
H-451 block graphite density (kg/m^3)	1,850	± 0.06%	[2]
Coated TRISO particles properties			
UC$_{0.5}$O$_{1.5}$ kernel diameter (μm)	425	± 2.58%	[1]
Buffer thickness (μm)	100	± 7.93%	[1]
IPyC thickness (μm)	40	± 5.84%	[1]
SiC thickness (μm)	35	± 3.69%	[1]
OPyC thickness (μm)	40	± 5.13%	[1]
UC$_{0.5}$O$_{1.5}$ kernel density (kg/m^3)	10,400	± 0.14%	[1]
Buffer density (kg/m^3)	1,050	± 3.64%	[1]
IPyC density (kg/m^3)	1,900	± 0.74%	[1]
SiC density (kg/m^3)	3,190	± 0.10%	[1]
OPyC density (kg/m^3)	1,900	± 0.42%	[1]

a. The uncertainty information in [1] originally only applied for NBG-18 graphite, but due to a lack of data for the TRISO coatings, the same variations are assumed for these materials at this stage.

Table C-6. Nuclide densities of the VHTRC fuel compact [5].

Item	Nuclide	Nuclide Density [at/b-cm]	
		B-2 Type	**B-4 Type**
Kernel of fuel particle[a]	^{234}U	3.1900E-06 ± 1.06%	7.5353E-06 ± 0.78%
	^{235}U	4.7058E-04 ± 1.06%	9.3498E-04 ± 0.78%
	^{236}U	3.7487E-07 ± 1.06%	5.8654E-06 ± 0.78%
	^{238}U	2.2764E-02 ± 1.06%	2.2143E-02 ± 0.78%
	^{16}O	4.6545E-02 ± 1.06%	4.6182E-02 ± 0.78%
	^{10}B	1.8481E-08	1.8357E-08
	^{11}B	7.4388E-08	7.3888E-08
1st coating layer of fuel particle	Graphite	5.9666E-02 ± 1.69%	5.9165E-02 ± 2.55%
	^{10}B	2.1106E-09	2.0929E-09
	^{11}B	8.4954E-09	8.4240E-09
2nd coating layer of fuel particle	Graphite	9.3761E-02 ± 1.07%	9.3761E-02 ± 1.07%
	^{10}B	3.3166E-09	3.3166E-09
	^{11}B	1.3350E-08	1.3350E-08
Matrix of graphite of fuel compact	Graphite	8.5715E-02 ± 1.17%	8.4712E-02 ± 1.19%
	^{1}H	3.2010E-05	3.1635E-05
	^{16}O	1.6005E-05	1.5818E-05
	^{10}B	3.0329E-09	2.9974E-09
	^{11}B	1.2208E-08	1.2065E-08

a. Uncertainties regarding the fuel are given for the enrichment, uranium content per compact, uranium isotope abundance, O/U atomic ratio, and UO$_2$ density. It was calculated that the uncertainties from the density is the largest of all (in %); thus, this value was chosen for this benchmark.

Table C-7. Nuclide densities of the VHTRC graphite sheath and other components [2].

Item	Nuclide	Nuclide Density [at/b-cm]
Graphite sheath for fuel rod[a]	Graphite	8.3925E-02 ± 3.05%
	^{10}B	1.2989E-09
	^{11}B	5.2284E-09
	^{1}H	1.2311E-05
	^{16}O	8.7794E-06
	^{14}N	9.7440E-06
	^{15}N	3.5598E-08
Other graphite components: reflector and fuel blocks, end caps for blocks, graphite rods (4 types), end cap for fuel rod	Graphite	8.3791E-02 ± 0.06%
	^{10}B	1.2969E-09
	^{11}B	5.2201E-09
	^{1}H	1.2291E-05
	^{16}O	8.7818E-06
	^{14}N	9.7890E-06
	^{15}N	3.5762E-08

a. Nitrogen and a part of the oxygen belong to air in pores. Because no information on the values of air is provided, uncertainties for ^{14}N and ^{15}N cannot be given. Furthermore, the uncertainty coming from moisture in graphite is assumed to be the only uncertainty for oxygen.

REFERENCES

1. J. T. Maki, *AGR-1 Irradiation Experiment Test Plan*, INL/EXT-05-00593, Rev. 3, 2009.

2   NEA, *Temperature effect on reactivity in VHTRC 1 core*, VHTRC GCR EXP 001, CRIT COEF, NEA/NSC/DOC(2006)2, 2006.

3. B. P. Collin and P. W. Humrickhouse, AGR-3/4 Irradiation Experiment Test Plan, PLN-3867, Rev. 0, October 2011.

4. G. Strydom, "TINTE Uncertainty Analysis of the Maximum Fuel Temperature during a DLOFC Event for the 400 MW Pebble Bed Modular Reactor," *Proceedings of ICAPP 2004, Pittsburgh, USA*, 2004.

5. NEA, "Temperature effect on reactivity in VHTRC 1 core," VHTRC GCR EXP 001, CRIT COEF, NEA/NSC/DOC(2006)2, 2006.

Appendix D

Calculation of Number Densities for Phase I

D-1. EXERCISE 1

For Exercise 1a, the fuel region in the unit cell is homogenized, i.e., the TRISO particles (consisting of the $UC_{0.5}O_{1.5}$ kernel and its coating layers) and the compact graphite matrix material are homogeneously distributed in this region. Graphite is a constituent in all particle layers and the matrix material, so that the total ^{12}C number density (ND) can be obtained by the sum of all the constituent ^{12}C NDs.

Using the average compact TRISO packing fraction of 0.35, the volume and number of TRISOs per compact can be calculated. This can be converted to the total number of atoms of a specific nuclide, and if this is divided by the compact volume, the NDs per nuclide are obtained. The data obtained for these few steps are shown in Table D-1 to Table D-5. The formulae used are shown below the tables.

Table D-1. TRISO and compact volumes and number of TRISOs per compact.

Description	Input Value/Unit	Result	Result Value/Unit
Compact radius	0.6225 cm	Compact volume	5.99928 cm^3
Compact length/height	4.9280 cm		
TRISO radius	4.2750E-02	TRISO volume	3.2726E-04
Compact-average TRISO packing fraction	0.35	No. of particles in compact	6,416 (integer rounded)

Table D-2. TRISO properties.

TRISO Layer	Radius (cm)	Vol. in Particle (cm^3)	Vol. in Compact (cm^3)
$UC_{0.5}O_{1.5}$ kernel	2.1250E-02	4.0194E-05	2.5789E-01
Porous carbon	3.1250E-02	8.7637E-05	5.6228E-01
IPyC	3.5250E-02	5.5639E-05	3.5698E-01
SiC	3.8750E-02	6.0257E-05	3.8661E-01
OPyC	4.2750E-02	8.3536E-05	5.3597E-01

Formulas used:

1. vol_comp: $V = h * \pi r^2$, with h = compact height, r = compact radius

2. vol_TRISO: $V = 4/3 * \pi r^3$, with r = TRISO radius

3. No._of_TRISO (per compact): $n = \frac{vol\_comp}{vol\_triso} * pack\_fract$, with $pack\_fract$ = packing fraction

4. vol_in_TRISO: $V = 4/3 * \pi r^3$, with r = $UC_{0.5}O_{1.5}$ kernel radius, or
   $V = \frac{4}{3} * \pi(r_2{}^3 - r_1{}^3)$, with r_1 = inner layer radius,
   r_2 = outer layer radius

5. vol_in_copmact: $V = vol_{in_{TRISO}} * \#\_of\_TRISO$, V= vol_in_TRISO*#_of_TRISOs

In the next step, the nuclide ND of the TRISO particles, $UC_{0.5}O_{1.5}$ kernel and SiC layer are calculated, since this is required as input to homogenization calculation.

Table D-3. Nuclide ND calculations for TRISOs.

Material	Molar Mass M (g/mol)	Mass Density ρ (g/cm³)	Nuclide ND N_D (1E24/cm³)
$UC_{0.5}O_{1.5}$ kernel	See Table D-4	10.40	See Table D-4
Buffer	12.0107	1.05	5.2646E-02
IPyC	12.0107	1.90	9.5263E-02
SiC	See Table D-5	3.19	See Table D-5
OPyC	12.0107	1.90	9.5263E-02
Graphite matrix	12.0107	1.45	7.2701E-02
H-451 block graphite	12.0107	1.85	9.2756E-02

Table D-4. Nuclide ND calculations for $UC_{0.5}O_{1.5}$ kernel.

Nuclide	Molar Mass M (g/mol)	x_i (atomic abundance)	Nuclide number density N_D (1E24/cm³)
^{235}U	235	0.15667	3.6676E-03
^{238}U	238	0.84333	1.9742E-02
^{16}O	15.9994	1.5	3.5114E-02
^{12}C	12.0107	0.5	1.1705E-02
Total	267.5344	—	—

Table D-5. Nuclide ND calculations for SiC layer.

Nuclide	Molar Mass M (g/mol)	x_i (atomic abundance)	Nuclide number density N_D (1E24/cm³)
^{28}Si	28	0.92223	4.4159E-02
^{29}Si	29	0.04685	2.2433E-03
^{30}Si	30	0.03092	1.4805E-03
^{12}C	12.0107	1.0	4.7883E-02
total	40.11939	—	—

Formulas used:

$$N_D = N_A \cdot \frac{\rho}{M} \qquad N_D = x_i \cdot N_A \cdot \frac{\rho}{M} \qquad at.-enr. = \frac{1}{1+\frac{1-enr}{enr}\cdot\frac{M^{U235}}{M^{238}}}$$

with

N_A	=	Avogadro constant 6.022E+23
ρ	=	mass density (g/cm³)
M	=	molar mass (g/mol)
x_i	=	atomic abundance
at. enr.	=	atomic enrichment
enr.	=	mass enrichment.

In the final homogenization step for Exercise I-1a, the number densities obtained above (as used for Exercise I-1b) are converted to the number density per compact (Table D-6).

Table D-6. Nuclide number density calculations.

Nuclide (component)	Nuclide number density N_D [1E24/cm^3]	No. Atoms per Compact	Homogenized number density N_D in compact [1E24/cm^3]
^{235}U (kernel)	3.6676E-03	9.4581E+20	1.5765E-04
^{238}U (kernel)	1.9742E-02	5.0912E+21	8.4864E-04
^{16}O (kernel)	3.5114E-02	9.0555E+21	1.5094E-03
^{28}Si (SiC)	4.4159E-02	1.7072E+22	2.8457E-03
^{29}Si (SiC)	2.2433E-03	8.6727E+20	1.4456E-04
^{30}Si (SiC)	1.4805E-03	5.7238E+20	9.5408E-05
^{12}C (kernel)	1.1705E-02	3.0185E+21	lumped into total ^{12}C
^{12}C (porous carbon)	5.2646E-02	2.9601E+22	lumped into total ^{12}C
^{12}C (IPyC)	9.5263E-02	3.4006E+22	lumped into total ^{12}C
^{12}C (SiC)	4.7883E-02	1.8511E+22	lumped into total ^{12}C
^{12}C (OPyC)	9.5263E-02	5.1058E+22	lumped into total ^{12}C
^{12}C (matrix)	7.2701E-02	2.8350E+23	lumped into total ^{12}C
^{12}C (total in compact)	—	4.1969E+23	6.9958E-02

D-2. EXERCISE 2

As a first step, the homogenized LBP compact details are calculated (Table D-7 and Table D-8). The homogenized number densities in the compact are calculated next, as shown in Table D-9.

Table D-7. LBP compact volumes and number of particles per compact.

Description	Input Value/Unit	Result	Result Value/Unit
Compact radius	0.5715 cm	Compact volume	5.0565 cm^3
Compact length/height	4.9280 cm		
Particle radius	1.4100E-02	Particle volume	1.1742E-05
Compact-average particle packing fraction	0.1090	Number of particles in compact	46,939 (integer rounded)

Table D-8. Particle properties.

TRISO Layer	Radius (cm)	Vol. in Particle (cm^3)	Vol. in Compact (cm^3)
Kernel	1.0000E-02	4.1888E-06	1.9662E-01
Buffer (^{12}C)	1.1800E-02	2.6935E-06	1.2643E-01
PyC (^{12}C)	1.4100E-02	4.8598E-06	2.2811E-01

Table D-9. Nuclide number density calculations.

Nuclide (component)	Nuclide number density N_D [1E24/cm^3]	No. Atoms per Compact	Homogenized number density N_D in Compact [1E24/cm^3]
^{10}B (kernel)	2.1400E-02	4.2076E+21	8.3211E-04
^{11}B (kernel)	8.6300E-02	1.6968E+22	3.3557E-03
^{12}C (kernel)	2.6900E-02	5.2890E+21	Lumped into total ^{12}C
^{12}C (buffer)	5.0200E-02	6.3469E+21	Lumped into total ^{12}C
^{12}C (PyC)	9.3800E-02	2.1397E+22	Lumped into total ^{12}C
^{12}C (matrix)	7.2700E-02	3.2754E+23	Lumped into total ^{12}C
^{12}C (total in compact)	—	3.6057E+23	7.1308E-02

In the next steps, the NDs for the fresh (Exercise I-2a) and burned fuel (Exercise I-2b) blocks are determined, as well as the data required for the supercell (Exercise I-2c) consisting of two depleted fuel blocks and one fresh fuel block on one side and reflector blocks on the other side. The embedded Excel sheet (Figure D-1) contains the calculation of these data sets.

number_densities_su
percell.xlsx

Figure D-1. Excel file: Homogenized region ND calculation for Exercise I-2c.

Appendix E

Summary of Changes

During the 2nd RCM held in Vienna on December 2–5, 2014, a number of changes were suggested by the participants to the previous version of the Phase I specifications. Table E-1 summarizes the main recommendations and resolutions implemented in this version of the Phase I specifications.

All previous calculations must be repeated, since significant changes were made.

Table E-1. Summary of Issues and Resolutions.

Change Request/Issue	Resolution/Comment
General	
Provide a list of changes made.	Included in this version onward.
Discussed at meeting: • Define material in PyC/SiC/matrix material as 100% graphite • Increase accuracy in number densities (NDs) • Explain the use of 600 K for CZP. Add a 300 K case.	• Error in SiC ND calculation corrected. • All ND digits increased from 2 to 4. • CZP temperature adjusted from 600 K to 293 K. • 293 K chosen to coincide with XS library point. • Moderator and fuel temperature equal for both CZP (293 K) and HZP (1,200 K). • All carbon treated as 100% graphite.
Provide the formulas used in the ND calculations.	Included in Appendix D.
Use of a one-group effective cross section.	Decision on a one- or two-group definition (as used in LWR UAM) deferred to a later point. Discussion and formulae used to determine sensitivity coefficients simplified.
Comparison of stand-alone or combined uncertainties.	Participants can perform three sub-cases: • Only cross-section uncertainties • Only manufacturing uncertainties • Both combined. Cross-section uncertainties are the main focus if only one option can be investigated.
Consideration of code/modeling uncertainties.	The code (e.g., mathematical formulations, numerical schemes) and modeling uncertainties (e.g., geometry and user approximations) cannot be quantified by this benchmark. They need to be assessed via verification and validation activities for each code. The CRP focuses on model input uncertainties only (cross sections, manufacturing).

Table E-1. (continued).

Change Request/Issue	Resolution/Comment
Exercises I-1 and I-2	
Correlated uncertainties in manufacturing data: • Are the fuel dimensions and layer thickness uncertainties correlated? • Do we implement this as variations in NDs or leave to participants to decide?	No clear resolution reached yet. In this specification version, the available physical input uncertainties (radii, packing fractions, enrichment loading, etc.) are converted to ND variations to ensure consistent interpretation by participants. Some of these parameters were derived from others, but the dependencies are not yet characterized.
Justification for doing Exercise I-1a?	Currently, still included in this version. We only start with this unrealistic case because we can learn from it and compare results before more complex treatments are required. With the lack of a DoubleHet treatment in the Sale 6.2 Beta 4/5 versions, this case can be used to explore other Sampler, for example. It has already been decided not to include Exercise1a in the final CRP report.
1. Propagate uncertainties from I-1 to I-2? 2. Exercise I-2b: Is performing the burnup calculation without burnable poisons okay? 3. Can we reduce the set of depleted nuclides? 4. Is a single supercell geometry sufficient, or do we need to look at more samples? 5. Group structure for propagation to core Phase II? 6. Group structure for comparison?	1. No. 2. Yes. 3. Yes. 4. Retained current geometry catered on Block 26, but INL to investigate other supercell geometries as well. Changed the previous definition to now include fresh/depleted contributions. 5. Participants to decide. OECD structure uses 26 groups, KAERI uses 13 groups, General Atomics uses nine groups, and Pennsylvania State University uses four groups. 6. One group only. If two groups are decided on, the thermal cutoff needs to be >3 eV.
Spectrum for Exercise 1 unit cell is too hard.	Not clear what, if any, effect this will have on uncertainties. A more representative cell definition that includes the pin and coolant channel (like Exercise I-3) was proposed and included here as Exercise I-1c/d.
No graphite impurities were defined.	No changes included in this version for fuel graphite, but the reflector graphite in Exercise I-2c includes Equivalent Boron-10 Content specification in reflector blocks. Suggest obtaining data from ASTRA facility to specify natural boron equivalent (or B-10), and perform a side study on Exercise I-1a. We can then add it to Exercise I-2a onward if significant. We should not deplete it. Can also cross check the OECD HTGR depletion benchmark (M. DeHart) on their treatment of this issue.
Exercises I-3 and I-4	
Do we need to include an effective gap conductance over the helium gap?	Some data could be obtained on the value used by the INL Advanced Test Reactor test irradiations, but it is unclear how representative it is for our problem (helium is not used). Further investigation is required for inclusion in Phase II as well.